~~Identifying Better~~ Assessing Potential Indicators of Aerosol Wet Scavenging During Long-Range Transport

Miguel Ricardo A. Hilario[1], Avelino F. Arellano[1], Ali Behrangi[1,2], Ewan C. Crosbie[3,4], Joshua P. DiGangi[3], Glenn S. Diskin[3], Michael A. Shook[3], Luke D. Ziemba[3], and Armin Sorooshian[1,5]

[1] Department of Hydrology and Atmospheric Sciences, University of Arizona, Tucson, AZ, USA
[2] Department of Geosciences, University of Arizona, Tucson, AZ, USA
[3] NASA Langley Research Center, Hampton, VA, USA
[4] Science Systems and Applications, Inc., Hampton, VA, USA
[5] Department of Chemical and Environmental Engineering, University of Arizona, Tucson, AZ, USA

Correspondence to: Armin Sorooshian (armin@arizona.edu)

Abstract. As one of the dominant sinks of aerosol particles, wet scavenging greatly influences aerosol lifetime and interactions with clouds, precipitation, and radiation. However, wet scavenging remains highly uncertain in models, hindering accurate predictions of aerosol spatiotemporal distributions and downstream interactions. In this study, we present a flexible, computationally inexpensive method to identify meteorological variables relevant for ~~to~~ estimating wet scavenging using a combination of aircraft, satellite, and reanalysis data augmented by trajectory ~~modeling~~modelling to account for air mass history. ~~Treating the enhancement (Δ) ratio of black carbon and carbon monoxide (ΔBC/ΔCO) measured by aircraft as an in situ proxy for wet scavenging, w~~We assess the capabilities of an array of meteorological variables to predict the transport efficiency of black carbon (~~ΔBC/ΔCO~~TE_{BC}) ~~-~~using a combination of nonlinear regression, ~~-statistics derived from~~ curve-fitting, and k-fold cross-validation. We find that accumulated precipitation along trajectories (APT) – treated as a wet scavenging indicator across multiple studies – ~~is unable to~~ does poorly when ~~accurately capture~~ predicting TE_{BC} ~~ΔBC/ΔCO trends, suggesting that APT is not a good indicator of wet scavenging effects~~. Among different precipitation characteristics (amount, frequency, intensity), precipitation intensity was the most effective at estimating TE_{BC} but required longer trajectories (> 48 h) and including only intensely precipitating grid cells. This points to the contribution of intense precipitation towards aerosol scavenging and the importance of accounting for air mass history. Predictors that were most able to predict TE_{BC} were related to the distribution of relative humidity (RH) or the frequency of humid conditions along trajectories, suggesting that RH is a more robust way to estimate TE_{BC} than APT. We recommend the following alternatives to APT when estimating aerosol scavenging: (1) the 90th percentile of RH along trajectories, (2) the fraction of hours along trajectories with either water vapor mixing ratios > 15 g kg^{-1} or RH > 95%, (3) precipitation intensity along trajectories at least 48 hours along and filtered for grid cells with precipitation > 0.2 mm h^{-1}. Future scavenging parametrizations should consider these meteorological variables along air mass histories.~~In contrast, the frequencies of precipitation or high relative humidity along trajectories better predict ΔBC/ΔCO trends and magnitudes, suggesting that these types of meteorological variables are better than APT for estimating the degree of wet scavenging in an air mass. Precipitation characteristics (e.g., intensity, frequency) from satellite retrievals are better indicators of ΔBC/ΔCO than those calculated from reanalysis, supporting previous studies that demonstrated reanalysis to be less reliable than satellite retrievals in terms of precipitation. Finally, top quantiles (e.g., 90th) of relative humidity are able to consistently capture the behavior of ΔBC/ΔCO and may also be a more suitable indicator of wet scavenging than APT. Future studies can use the best-performing meteorological variables identified in our study to estimate wet scavenging. Furthermore,~~ T~~t~~his method can be repeated for different regions to identify ~~region-specific~~ region-specific factors influencing wet scavenging~~, and our findings may be useful for informing scavenging parametrization schemes in models~~.

Formatted: Subscript

Formatted: Subscript

Formatted: Superscript

Formatted: Superscript

Formatted: Superscript

1 Introduction

Although wet scavenging is one of the dominant removal mechanisms for atmospheric aerosol particles (Seinfeld and Pandis, 2016; Textor et al., 2006), it remains a large source of uncertainty in global-scale models (Watson-Parris et al., 2019; Liu and Matsui, 2021; Moteki et al., 2019; Hodzic et al., 2016). This uncertainty hampers the ability of global-scale models to capture the lifecycle (i.e., sources, transformations, and sinks) (Hou et al., 2018), spatial extent (Moteki et al., 2019), and vertical profile (Watson-Parris et al., 2019; Liu and Matsui, 2021; Frey et al., 2021; Kipling et al., 2016) of aerosol particles. Inaccurate representations of these aerosol features contribute to uncertainties in estimates of aerosol radiative effects (Samset et al., 2013; Marinescu et al., 2017) and aerosol loadings over climate-sensitive regions (Liu and Matsui, 2021; Mahmood et al., 2016; Shen et al., 2017), with further implications for the remote sensing of aerosol abundance downwind of precipitating or cloudy areas. Advancing knowledge of wet scavenging processes can help reduce the largest uncertainty in human forcing of the climate system, which involves aerosol-cloud interactions (e.g., Bellouin et al., 2020).

Wet scavenging occurs either below- or in-cloud. Below-cloud scavenging occurs when aerosol particles are collected by precipitation (Croft et al., 2009) and is most important between the surface and 1 km above ground level (AGL) (Grythe et al., 2017). The efficiency of below-cloud scavenging depends on raindrop size distributions (Wang et al., 2010), ~~and~~ aerosol composition (Lu and Fung, 2018; Grythe et al., 2017), the amount of in-cloud condensed water (Luo et al., 2019) as well as precipitation characteristics (i.e., frequency, intensity, amount, and type) ~~the amount of in-cloud condensed water (Luo et al., 2019)~~. To calculate the fraction of aerosol scavenged below-cloud, models typically rely on an empirically-derived below-cloud scavenging coefficient, which is a function of aerosol size (Feng, 2007; Croft et al., 2009) and composition (Lin et al., 2021). Semi-empirical model parametrizations of below-cloud scavenging have been shown to improve simulated surface concentrations (Luo et al., 2019); however, agreement between models and observations is highly sensitive to the specific below-cloud scavenging scheme used (Lu and Fung, 2018). Below-cloud scavenging rates in models also remain significantly underestimated compared to observations (Kim et al., 2021; Ryu and Min, 2022; Xu et al., 2019).

~~(~~Wang et al. (~~,~~2010) determined the below-cloud scavenging coefficient is influenced by (1) raindrop-particle collection efficiency, (2) raindrop size distribution, and (3) raindrop terminal velocity. These factors were associated with differences in particle concentrations by a factor of 2 for sub-10 nm particles and a factor of >10 for particles larger than 3 μm; however, their combined uncertainty was insufficient to explain the discrepancy between theoretical and field measurements of the below-cloud scavenging coefficient. ~~(~~Wang et al. (~~,~~2011) demonstrated that this discrepancy can be largely explained by the vertical turbulence as it determines which particles are subjected to impaction scavenging. This impact was most pronounced for submicron particles under weak precipitation intensities.

Given these uncertainties, ~~(~~Wang et al. (~~,~~2014a~~b~~) ~~(Wang et al., 2014b)~~developed a new semi-empirical, size-resolved parametrization based on an percentile-logarithmic power-law relationship between the below-cloud scavenging coefficient and particle size that is applicable to both rain and snow across different particle sizes and precipitation intensities. Based on the size-resolved parametrization of ~~(~~Wang et al. (~~,~~2014a~~b~~), ~~(Wang et al., 2014a)(Wang et al., 2014a)~~a bulk or modal parametrization for fine ($PM_{2.5}$), coarse ($PM_{2.5-10}$), and giant particles (PM_{10+}) was presented by Wang et al. (2014b).

Formatted: Subscript

Formatted: Subscript

Formatted: Subscript

In-cloud scavenging occurs via nucleation (i.e., activation of aerosol particles into cloud droplets; Jensen and Charlson, 1984) or impaction (i.e., collision of interstitial aerosol particles with existing cloud droplets; Kipling et al., 2016; Flossmann et al., 1985) and is followed either by (1) precipitation that reaches the surface, removing the particle from the atmosphere (Radke et al., 1980), or (2) evaporation of cloud droplets or precipitation, returning the scavenged particle to the free atmosphere (Mitra et al., 1992). Model improvements in in-cloud scavenging include using a continuous rather than binary cloud fraction (Ryu and Min, 2022; Xu and Randall, 1996), accounting for cloud water phase (Grythe et al., 2017; Liu and Matsui, 2021), and accurately simulating cloud supersaturation (Moteki et al., 2019). Although in-cloud scavenging is generally thought to be more efficient at removing accumulation mode aerosol particles (Watson-Parris et al., 2019; Choi et al., 2020), other studies argue that there are instances wherein below-cloud scavenging becomes more important at regulating aerosol burdens (Kim et al., 2021; Ryu and Min, 2022; Xu et al., 2019). Uncertainties related to wet scavenging are further exacerbated by the divergent role of clouds, which can be a sink or source of aerosol particles depending on environmental factors and cloud characteristics (Ryu et al., 2022).

One avenue for improving the estimation of wet scavenging, particularly in observational studies, is to identify an effective meteorological indicator of wet scavenging. Previous studies used precipitation amount (Feng, 2007; Andronache, 2003) while more recent studies accounted for air mass history using the National Oceanic and Atmospheric Administration (NOAA) Hybrid Single Particle Lagrangian Integrated Trajectory Model (Rolph et al., 2017; Stein et al., 2015) to calculate accumulated precipitation along trajectories (APT) (e.g., Kanaya et al., 2016, 2020). However, APT can be problematic as an indicator of wet scavenging because APT is an accumulated quantity and does not consider specific characteristics of precipitation relevant to scavenging such as intensity and frequency (Hou et al., 2018; Wang et al., 2021~~c, b~~b, c; Hilario et al., 2022). APT as an indicator of wet scavenging also relies on the correct detection of precipitation and retrievals of amounts, which are challenging during both light (Nadeem et al., 2022; Kidd et al., 2021) and intense precipitation events (Chen et al., 2020a; Gupta et al., 2020) and even show disagreements between different satellite precipitation products (SPPs) and reanalyses (Cannon et al., 2017; Jiang et al., 2021; Alexander et al., 2020; Chen et al., 2020b; Barrett et al., 2020). Furthermore, precipitation from SPPs such as the Precipitation Estimation from Remotely Sensed Information using Artificial Neural Networks – Climate Data Record (PERSIANN-CDR) (Ashouri et al., 2015; Nguyen et al., 2018) and the Integrated Multi-satellitE Retrievals for the Global Precipitation Measurement (GPM) mission (IMERG) (Huffman et al., 2020) refer to total column precipitation that have been validated mainly with surface measurements (Sapiano and Arkin, 2009; Nicholson et al., 2019; Wang et al., 2021a) and consequently may not detect precipitation that evaporates before reaching the surface (e.g., virga) (Wang et al., 2018).

Given the uncertainties of estimating wet scavenging from precipitation, we present a flexible, computationally inexpensive method to identify alternative meteorological variables that can be used to better estimate wet scavenging. We combine curve-fitting and k-fold cross-validation to evaluate an array of meteorological variables from aircraft, satellite, and reanalysis data to answer the following:

(1) What meteorological variables can estimate wet scavenging trends better than APT? Since precipitation frequency has been shown to exert significant control over aerosol scavenging (Wang et al., 2021b), we hypothesize that predictors that account for the frequency of scavenging-conducive conditions (e.g., frequency of high relative humidity (RH) conditions along trajectories) will be able to capture wet scavenging trends better than APT.

(2) How can APT be filtered or changed to better estimate wet scavenging? We hypothesize that considering precipitation intensity and/or trajectory altitude thresholds when calculating APT will improve its ability to estimate wet scavenging. We also hypothesize that calculating APT using SPPs will perform better than APT from reanalysis.

The presented method may be repeated over different regions to identify region-specific wet scavenging indicators. This can inform scavenging parameterization development for models by providing guidance on what meteorological variables are needed to properly capture wet scavenging processes over a specific region. Future studies can also use the best-performing variables identified in this study as alternatives to APT when estimating the extent of wet scavenging.

2 Data & Methods

2.1 Aircraft data

Much of the methodology and instrument details in this study are detailed elsewhere (Hilario et al., 2021) but are summarized here. We utilize aircraft measurements from NASA's Cloud, Aerosol, and Monsoon Processes-Philippines Experiment ($CAMP^2Ex$; 24 August to 5 October 2019) over the tropical West Pacific (5 – 20°N, 117 – 127°E) (Reid et al., 2023), which hosts a dynamic transport environment rich in aerosol sources and cloud-precipitation systems.

Black carbon (BC)-equivalent concentrations (particle diameters: 100 – 700 nm; units: µg m^{-3}) were measured with a Single-Particle Soot Photometer (SP2) (Moteki & Kondo, 2007, 2010) with an uncertainty of 15% (Slowik et al., 2007) and lower detection limit of 10 ng m^{-3} verified by filter-blank measurements as well as observations in the clean free troposphere. To eliminate in-cloud sampling artifacts such as droplet shattering on the inlet (Murphy et al., 2004), we use only data collected outside of clouds. All BC concentrations are reported at standard temperature and pressure (273 K, 1013 hPa). Carbon monoxide (CO; ppm) was measured using a dried-airstream near-infrared cavity ringdown absorption spectrometer (G2401-m; PICARRO, Inc.), with an uncertainty of 2% and precision of 0.005 ppm. As an in situ (i.e., at the aircraft's position) contrast to moisture-based variables along trajectories, relative humidity ($RH_{W,\ DLH}$) was derived from absolute water vapor concentrations that were retrieved by a diode laser hygrometer (DLH) (Livingston et al., 2008) on the aircraft.

2.2 Calculation of e~~E~~nhancement ratios~~ calculation~~

To relate wet scavenging to meteorological conditions during transport~~ conditions~~, previous studies ~~used ~~calculated enhancement (Δ) ratios of BC and ~~carbon monoxide~~CO ~~(CO)~~ (ΔBC/ΔCO; Hilario et al., 2021; Kanaya et al., 2016; Oshima et al., 2012) which can then be used to quantify the transport efficiency of BC (TE_{BC}) (Kanaya et al., 2016, 2020; Oshima et al., 2012), discussed more in Sect. 2.5.~~ ~~By using the enhancement above a local background, ΔBC/ΔCO accounts for ~~spatial variations in the~~ background ~~levels ~~concentrations of BC and CO at a receptor site ($\left(\frac{\Delta BC}{\Delta CO}\right)_{receptor}$) and is better able to detect a transported~~n~~ air mass containing BC and CO above local background levels. This ratio can be used as an indicator of wet scavenging because BC is relatively chemically inert and is mainly removed from the atmosphere via wet scavenging (Moteki et al., 2012). While CO is also relatively chemically inert, CO has a lifetime between 30 to 90 days (Seinfeld and Pandis, 2016) that is mainly controlled by photochemistry rather than wet scavenging due to its low solubility. ~~Because of this, we use ΔBC/ΔCO as our proxy for wet scavenging and the predictand for our regression models.~~

Enhancements were defined as the difference between species concentrations and the lowest 5^{th} percentile species concentration for all $CAMP^2Ex$ data for every 5 K potential temperature bin (Koike et al., 2003; Matsui et al., 2011). As $CAMP^2Ex$ spanned the late southwest monsoon and early monsoon transition, background concentrations (i.e., lowest 5^{th} percentile) were calculated for each monsoon phase using 20 September 2019 to divide the two monsoon phases. Only data with ΔCO > 0.02 ppm were included to reduce uncertainties caused by low denominator values in the ΔBC/ΔCO ratio (Kleinman et al., 2007; Kondo et al., 2011; Matsui et al., 2011). When calculating transport efficiency (Sect. 2.5), we converted ΔCO (from the receptor) from ppm to µg m^{-3} using the ambient pressure and temperature measured by the aircraft such that ΔBC/ΔCO would be unitless.

As ΔBC/ΔCO is expected to vary by source region, Fig. S1a shows source-resolved distributions of ΔBC/ΔCO (unitless) based on source regions identified by ~~(~~Hilario et al. (~~, ~~2021), which classified backward trajectories into source regions using bounding boxes over major source regions established in previous literature. In addition to passing over source region bounding boxes, the source classification also considered (1) trajectory altitude, specifically whether or not the trajectory was below 2 km AGL which

Formatted: Subscript

Formatted: Font color: Auto

Formatted: Font color: Auto

Formatted: Font color: Auto

Formatted: Not Highlight

Formatted: Not Highlight

conservatively approximates climatological boundary layer heights over the region (Chien et al., 2019), as well as (2) trajectory residence time within each bounding box (minimum residence time: 6 hours). As described in Hilario et al. (2021), ΔBC/ΔCO is higher for air masses coming from East Asia or the Maritime Continent (Fig. S1a), which suggests a low degree of aerosol scavenging during transport, while lower ΔBC/ΔCO are seen for air from the Peninsular Southeast Asia, indicating scavenging had occurred~~(Hilario et al., 2021)~~. More information on major transport patterns affecting BC and CO during CAMP^{2}Ex are provided in Appendix A.

2.3 Trajectory modeling

Trajectory modeling is a computationally inexpensive tool for characterizing transport processes (Kanaya et al., 2016; Oshima et al., 2012; Moteki et al., 2012) and has been used in synergy with aircraft data (Hilario et al., 2021; Dadashazar et al., 2021). In this study, we use trajectories to account for meteorological conditions during air parcel transport that are expected to impact the scavenged aerosol fraction. Backward trajectories were spawned every minute along the aircraft flight path and run for 72 hours using the NOAA HYSPLIT model. Meteorological input data for the HYSPLIT model were from the National Centers for Environmental Prediction (NCEP) Global Forecast System reanalysis (GFS; 0.25° × 0.25°). Figure S1b shows the distribution of transport times from different source regions (Sect. 2.2) to the CAMP^{2}Ex aircraft~~(Hilario et al., 2021)~~. Generally, transit times are below 72 hours, indicated by 25th and 75th percentiles less than 72 hours, suggesting that 72 hours is sufficient to capture long-range transport from major source regions into the tropical West Pacific.~~(Chien et al., 2019)~~

2.4. Emission inventory

To calculate the BC/CO emission ratio over each trajectory ($ER_{BC/CO}$), we used data from the Copernicus Atmosphere Monitoring Service (CAMS) Global Anthropogenic Emissions (CAMS-GLOB-ANT) inventory, version 5.3 (Soulie et al., 2023) which is based on the Emissions Database for Global Atmospheric Research (EDGAR) inventory from the European Joint Center (Crippa et al., 2018) and the Community Emissions Data System (CEDS) from the Joint Global Research Institute (Hoesly et al., 2018). CAMS-GLOB-ANT has a horizontal resolution of 0.1~~x~~ × 0.1° at monthly resolution. CAMS-GLOB-ANT accounts for 17 emission sectors, including shipping from CAMS-GLOB-SHIP v3.1, and emissions are reported in units of mass flux (kg m^{-2} s^{-1}). ~~(Crippa et al., 2018)(Hoesly et al., 2018)~~More information on CAMS global and regional emissions can be found in (Granier et al. (~~,~~ 2019).

2.5. Calculation of transport efficiencies

The TE_{BC} (unitless) was calculated for each trajectory using Eq. 1:

$$TE = \frac{\left(\frac{\Delta BC}{\Delta CO}\right)_{receptor}}{ER_{BC/CO}} \qquad (1)$$

w~~W~~here $\left(\frac{\Delta BC}{\Delta CO}\right)_{receptor}$ is the enhancement ratio calculated from the aircraft data (Sect. 2.2) and $ER_{BC/CO}$ is the weighted-average emission ratio of BC/CO along each 72-h trajectory, inverse-weighted by altitude and calculated using emissions from the CAMS-GLOB-ANT inventory (Sect. 2.4). When calculating $ER_{BC/CO}$ for each trajectory, we applied a weighting function (Fig. S2a) to assign higher weights to lower altitudes such that the resulting $ER_{BC/CO}$ will be mainly determined by times when trajectory altitude is low, reflecting the higher likelihood of entraining surface emissions when the trajectory is close to the

Formatted: Not Highlight
Formatted: Superscript
Formatted: Body Text, Indent: First line: 0.18", Right: 0.08", Line spacing: Multiple 1.3 li
Formatted: Not Highlight
Formatted: Not Highlight
Formatted: Superscript
Formatted: Superscript
Formatted: Superscript
Formatted: Subscript
Formatted: Font: 10 pt
Formatted: Font: 10 pt
Formatted: Font: 10 pt
Formatted: Font: 10 pt
Formatted: Indent: First line: 0"

surface. An example of the weighting function as a function of trajectory altitude is shown in Fig. S2b wherein weighting decreases with increasing trajectory altitude. As the $ER_{BC/CO}$ calculation included the entire 72 hour length of the trajectory, our method of computing $ER_{BC/CO}$ is not restricted only to source regions (e.g., East Asia) but also accounts for potential entrainment of BC or CO over the open ocean, where sources such as shipping could contribute BC (Lack and Corbett, 2012) and CO (Jalkanen et al., 2012). We note that $ER_{BC/CO}$ is not required to be an enhancement ratio because the purpose of the enhancement ratio is to account for local background concentrations over the receptor region (Sect. 2.2).

We found that TE_{BC} and ΔBC/ΔCO are strongly correlated ($R^2 = 0.90$); however, TE_{BC} has the added advantage of accounting for surface emissions of BC and CO that could have been entrained into transported air mass. ΔBC/ΔCO is assumed to be influenced by two main factors: (1) source emissions of BC and CO along the trajectory path, and (2) removal of BC via wet scavenging. By setting TE_{BC} as our predictand, we account for emissions encountered during long-range transport ($ER_{BC/CO}$) such that TE_{BC} is expected to vary mainly via sinks (i.e., wet scavenging).

~~(Lack and Corbett, 2012)(Jalkanen et al., 2012)~~To show the variation of $ER_{BC/CO}$ and TE_{BC} with different source regions, Fig. S1 shows source-resolved $ER_{BC/CO}$ (Fig. S1c) and TE_{BC} (Fig. S1d). Air masses from East Asia show the smallest range in $ER_{BC/CO}$ while air masses from the Maritime Continent and Peninsular Southeast Asia have largely similar distributions. Lower values of $ER_{BC/CO}$ in air masses from the Maritime Continent are related to smoke from agricultural burning that coincided with the CAMP^{2}Ex period (Ge et al., 2014). Previous emission factor measurements showed that these fires tended to be smoldering rather than flaming, emitting CO but notably lower BC (Stockwell et al., 2015). ~~(Stockwell et al., 2015)(Ge et al., 2014)~~While some variation is indeed present between source regions, the distributions of $ER_{BC/CO}$ are generally similar with modes between 0.22 – 0.26, which may explain the strong correlation between TE_{BC} and ΔBC/ΔCO.

~~2.4~~2.6 Data for predictor variables

Several meteorological variables (i.e., predictors) considered in this work were calculated from GFS reanalysis collocated along each trajectory. Though reanalysis is relatively coarse and not cloud-resolving, reanalysis variables (e.g., RH) may still be useful in detecting the presence of meso-to-synoptic-scale cloud fields. As precipitation is expected to be accompanied by elevated RH or water vapor mixing ratio (MR), these reanalysis-derived variables could serve as effective scavenging indicators in cases where precipitation may be missed or misestimated.

In addition to APT from GFS, we calculated APT from two SPPs: PERSIANN-CDR (0.25° × 0.25°, daily resolution) (Ashouri et al., 2015; Nguyen et al., 2018) and IMERG Final v6 (0.1° × 0.1°, 30-min resolution) (Huffman et al., 2020). We converted precipitation from these products to hourly amounts to match trajectory timesteps prior to further calculation.

Besides APT, we also calculated precipitation amount (PA; mm h^{-1}), frequency (PF), and intensity (PI; mm h^{-1}), which are well-established in the literature for characterizing precipitation, particularly in diurnal cycle analyses (e.g., Zhang et al., 2017; Hilario et al., 2020). Applying these quantities to precipitation along trajectories, PA is APT divided by the total number of hours along the trajectory (i.e., trajectory length) to obtain an average hourly precipitation rate, PF is the fraction of hours along the trajectory where the grid cell precipitation is above 0 mm h^{-1}, and PI is the ratio of PA to PF. Table 1 shows notation used to explain each type of predictor and its variations.

~~2.5~~2.7 Curve-fitting and k-fold cross-validation

To quantify relationships between ~~ΔBC/ΔCO~~TE_{BC} and each predictor as well as its uncertainty, we performed k-fold cross-validation (k = 10) parallelized using the Python package ~~J~~jug, ~~-~~version 2.2.2 (Coelho, 2017). ~~This procedure was repeated for k iterations using a different partition for the testing set in each iteration, which provides a measure of uncertainty in the resulting regression statistics.~~

Formatted: Not Highlight
Formatted: Not Highlight
Formatted: Indent: Left: 0.07", First line: 0.18"
Formatted: Font color: Auto
Formatted: Font color: Auto
Formatted: Font color: Auto
Formatted: Font color: Auto
Formatted: Font color: Auto
Formatted: Font: 10 pt, Font color: Auto
Formatted: Font: 10 pt, Font color: Auto
Formatted: Font: 10 pt, Font color: Auto
Formatted: Font: 10 pt, Font color: Auto
Formatted: Font: 10 pt, Subscript
Formatted: Font: 10 pt, Font color: Auto
Formatted: Font: 10 pt, Font color: Auto
Formatted: Font: 10 pt
Formatted: Body Text, Indent: First line: 0.18", Right: 0.08", Line spacing: Multiple 1.3 li
Formatted: Font: 10 pt, Font color: Auto
Formatted: Font: 10 pt
Formatted: Font: 10 pt, Font color: Auto
Formatted: Font: 10 pt, Font color: Auto
Formatted: Font: 10 pt, Font color: Auto
Formatted: Font: 10 pt, Font color: Auto
Formatted: Font: 10 pt
Formatted: Font: 10 pt, Font color: Auto
Formatted: Font: 10 pt, Not Highlight
Formatted: Font: 10 pt
Formatted: Font: 10 pt, Font color: Auto
Formatted: Font: 10 pt, Subscript
Formatted: Font color: Blue
Formatted: Outline numbered + Level: 2 + Numbering Style: 1, 2, 3, … + Start at: 6 + Alignment: Left + Aligned at: 0.25" + Indent at: 0.5"
Formatted: Superscript
Formatted: Outline numbered + Level: 2 + Numbering Style: 1, 2, 3, … + Start at: 6 + Alignment: Left + Aligned at: 0.25" + Indent at: 0.5"
Formatted: Subscript

To create k distinct partitions of the data, we utilized stratified random sampling wherein random sampling was performed for ~~every~~ each 5th percentile block of the predictor such that the sampling probability better reflects the distribution of predictor values, which is ~~(e.g.,~~ important for skewed distributions such as precipitation amount, ~~)~~ and the resulting k partitions capture ~~s~~ the behavior of TE_{BC} ~~ABC/ΔCO over~~ across the ~~whole range~~ full spectrum of predictor values. By randomly sampling each percentile block for k distinct partitions, this sampling method improves the chances of capturing intra-block variability in ~~ABC/ΔCO~~TE_{BC} by collecting the most samples where the ~~most~~ highest data coverage exists. The random nature of the sampling also allows for the consideration of extreme values in the curve-fitting, with a sampling probability proportional to the frequency of these extreme values. As an example, Fig. 1a-b shows the emphasis of the stratified random sampling method on high density areas of the scatterplot of RH_{q90} and TE_{BC}~~ABC/ΔCO~~, denoted by dense percentile blocks (gray dashed lines). For extremely skewed distributions such as APT, several of the lower-value percentiles exhibited non-unique values (e.g., zero). In the case of repeated percentile values, these percentile-based groups were merged. We imposed a minimum of six distinct percentile blocks to ensure robust curve-fitting.

An iterative train-test split procedure using these partitions was then performed using ~~nine~~ k-1 partitions as the training set and the remaining ~~–~~ partition as the testing set (Fig. 1a). For each iteration of the k-fold cross-validation, nonlinear least squares curve-fitting was applied to the training set (i.e., 9 partitions for a total k of 10)~~,~~ to determine coefficients for the equation (e.g., general exponential; discussed below) fitted onto the scatterplot of TE_{BC} ~~ABC/ΔCO~~ and the predictor. We used these coefficients and the testing set (i.e., the remaining partition) as inputs for the curve-fitting equation and calculated a predicted curve of TE_{BC} ~~ABC/ΔCO~~ and the predictor. To assess this predicted curve, we applied stratified random sampling on the testing set and took the median TE_{BC} ~~ABC/ΔCO~~ per 5th percentile block to create observed curves of TE_{BC} ~~ABC/ΔCO~~ as a function of the predictor that could be compared to the predicted curve (Fig. 1b). Because decreases in TE_{BC} ~~ABC/ΔCO~~ are expected to be mainly from wet scavenging, the overall trend or median curve may be treated as a reasonable indicator of wet scavenging effects on TE_{BC} ~~ABC/ΔCO~~ related to changes in the predictor value.

Using a linear regression of predicted and observed median TE_{BC} ~~ABC/ΔCO~~ per 5th percentile block of the predictor (Fig. 1c), we calculated statistics (e.g., slope, R) to describe ~~the performance of the~~ how well the predictor can predict TE_{BC}~~(e.g., slope, R)~~. Specifically, ~~Note that~~ the performance of a predictor refers to how well TE_{BC} ~~ABC/ΔCO~~ derived from the predictor matches observed TE_{BC}~~ABC/ΔCO~~. We also computed statistics comparing predicted and observed TE_{BC} ~~ABC/ΔCO~~ for individual points (Fig. 1d) rather than medians to assess how much variability in TE_{BC} ~~ABC/ΔCO~~ is captured by the predicted curves. The population in Fig. 1d visually follows the 1-to-1 line, indicating good performance of the model; however, the best-fit line on individual points was greatly affected by outlier points of high observed TE_{BC} that led to poor agreement between the best-fit and 1-to-1 lines when the actual agreement was much better (visually). This suggests that the median-based statistics (Fig. 1c) are more robust to outliers and present a fairer evaluation of model predictions. Note that ~~These i~~the individual-point statistics (Fig. 1d) resulted in correlations and slopes further from ideal values compared to the median-based statistics. This is expected as individual TE_{BC} data ~~ABC/ΔCO~~ points ~~have~~ exhibit ~~high~~ large variability due to the influence of factors other than wet scavenging; however, a ~~comparison of~~ comparison of our results when using individual-point ~~and~~ or the median-based statistics show that they ~~qualitatively~~ agree quite well qualitatively, with the relative ranking of predictors largely unchanged between the two types of statistics. In other words, the top predictors performed well whether we used median-based or individual-point statistics, implying the conclusions reached using our method are qualitatively ~~unaffected~~insensitive to this choice. For simplicity, reported statistics in this study refer to median-based statistics unless otherwise specified.

To determine if a predict~~ed ABC/ΔCO curve tended to~~or tended to overestimate or underestimate ~~observed~~ TE_{BC}~~ABC/ΔCO~~, we calculated a weighted area difference (WAD) using Eq. 1:

Formatted: Not Superscript/ Subscript

Formatted: Subscript

$$WAD = \frac{\sum N_i \cdot x_i}{\sum N_i} \tag{1}$$

where x_i is the difference between observed and predicted TE_{BC} ~~ΔBC/ΔCO~~ for the i^{th} percentile block and N_i is the number of data points in that percentile block. A positive (negative) WAD indicates an overestimate (underestimate) of observed TE_{BC}~~ΔBC/ΔCO~~.

To account for differing relationships between TE_{BC} ~~ΔBC/ΔCO~~ and each predictor, we ~~fitted~~ applied curve-fitting on the ~~their~~ scatterplot of each predictor and TE_{BC} using multiple nonlinear equations (Table 2) and chose the equation that produced ~~ing~~ the highest Pearson correlation (R) between observed and predicted TE_{BC} ~~ΔBC/ΔCO~~ for that predictor. We considered equations from two previous studies (Kanaya et al., 2016; Oshima et al., 2012) and two generalized equations (Gaussian, general exponential) to capture other types of relationships (Table 2). The inclusion of the latter two are to account for a wider range of possible relationships between predictors and TE_{BC}, such as the case of a predictor capturing TE_{BC} trends well but not having an inversely proportional relationship with ΔBC/ΔCO. The case of a non-inversely proportional relationship with TE_{BC} is still interesting because a strong relationship implies that the variable could be used to estimate TE_{BC} even if their relationship is nonmonotonic. The final assigned equations led to similar root mean squared error (RMSE) across predictors (Fig. S3) suggesting it is fair to compare different predictors.

When selecting which equation to use (among those in Table 2) for fitting between the predictor and TE_{BC}, w~~W~~e opted ~~use~~ for the equation that resulted in the highest R between observed and predicted TE_{BC} (e.g., Fig. 1c). The basis of this choice on R was because ~~we are more interested in~~ our objective is to identify predictors that can at least capture trends in TE_{BC}~~ΔBC/ΔCO rather than magnitudes~~. After selecting which equation to use per predictor, the subsequent comparison (Sect. 3) of the performance of different predictors considers other statistical metrics such as slope, intercept, and WAD. For some combinations of predictors and ~~curve-fitting~~ equations, the curve-fitting did not successfully converge (< 4% of all combinations and k-fold iterations). In these cases, we did not include the predictor-equation combination in our analysis. However, curve-fitting on the predictor may still converge when using a different equation. In such a scenario, the predictor becomes part of our analysis.

~~This procedure was repeated for k iterations using a different partition for the testing set in each iteration, which provides a measure of uncertainty in the resulting regression statistics.~~ Sensitivity testing with the k value showed no significant effect on the general conclusions of the study when k was changed between 5 and 20 (not shown). We opted for k = 10 based on previous work evaluating different accuracy estimation methods which showed that k = 10 is sufficient to estimate performance metrics (e.g., R^2) while minimizing computational expense (Breiman and Spector, 1992; Kohavi, 1995).

Although there is no physical process built into this procedure, the strength of the method is its repeatability in different environments or regions with minimal changes to the overall procedure. As it requires no physical model to be run besides the trajectory calculations, the method is also relatively computationally inexpensive. Future work wanting a more physical basis may apply our method as a diagnostic tool to identify and narrow down a list of meteorological variables that may be relevant to wet scavenging and continue their analysis with a physical model using the narrowed list of variables to analyze.

3 Results and Discussion

3.1 Overall statistical performance

Figures 2, ~~-~~3, and S3 show performance comparisons of different predictors derived from linear regressions of observed and predicted ~~ΔBC/ΔCO~~TE_{BC}. Hereafter, the performance of a predictor in this study refers to a predictor's ability to ~~reproduce~~ predict

Formatted: Font: Not Italic

Formatted: Font color: Auto

Formatted: Font color: Auto

Formatted: Font color: Auto

Formatted: Font color: Auto

Formatted: Subscript

observed ~~$\Delta BC/\Delta CO$~~TE_{BC} ~~via~~ based on curve-fitting (Sect. 2.~~5~~7; Fig. 1c). To simplify these figures, only the top eight predictors per panel (by R) are ~~A threshold of Pearson R > 0.71 (R^2 > 0.50)~~ colored ~~was used to narrow~~ to focus our ~~analysis~~ discussion ~~to~~ on predictors that were able to ~~produce~~ predicted ~~$\Delta BC/\Delta CO$~~TE_{BC} ~~that captured trends in observed $\Delta BC/\Delta CO$~~. Table S1 provides the equation and coefficients used for the top eight predictors per panel of Fig. 2.

~~We note that~~ Using ~~no~~ APT-~~related~~ based predictors (Fig. 2a) ~~met this R threshold~~ led to moderate R between predicted and observed TE_{BC} but slopes far below the ideal value of 1, which, in addition to positive intercepts and WAD (Fig. S3a), indicate that APT-based predictors tend to underestimate TE_{BC} when APT is high.

In comparison, predictors in Fig. 2b are based on RH (e.g., f_{RH95}, RH_{q90}) or MR (i.e., f_{MR15}) and predicted TE_{BC} much better in terms of trends (high R) and magnitude (slopes close to 1), suggesting that these predictors (Fig. 2b) could be better at estimating TE_{BC} than APT (Fig. 2a) ~~may not be a good predictor of $\Delta BC/\Delta CO$ and, by extension, aerosol scavenging~~. One ~~explanation~~ possibility for this is that APT is an accumulated value that does not account for ~~different precipitation characteristics such as precipitation~~ frequency or intensity, both of which have been argued to be important for regulating aerosol scavenging (Hou et al., 2018; Wang et al., 2021c). To explore this possibility further, we calculated PA, PF, and PI for each trajectory (Figs. 2c-e~~Sect. 2.4~~). Among these three, PF (Fig. 2d) and ~~PF~~ PI (Fig. 2e) resulted in ~~the most predictors satisfying the minimum R of 0.71~~ the best slopes and R, with PI showing slightly better slopes and R than PF. In comparison, PA performed poorly, similar to APT, which is expected as both are related to summed precipitation amount. Comparing the PI variables with the highest R (i.e., colored points in Figs. 2e), the majority of these good-performing PI variables were filtered for heavier or more intense precipitation (i.e., > 0.2 mm). This filtering for heavier precipitation was done by including only grid cells with precipitation > 0.2 mm when calculating PI. A similarly good performance was observed for PF variables that also filtered for more intense precipitation. ~~Several PF-related variables in Fig. 2 have R over 0.71, even when accounting for the 25th and 75th percentile error bars derived from k-fold cross-validation. In comparison, only one PA-related predictor ($PA_{48H, IMERG}$; Fig. 2a) and one PI-related predictor ($PI_{PCP > 0.2mm, 48H, P-CDR}$; Fig. 2b) pass the R > 0.71 threshold, which indicates that $\Delta BC/\Delta CO$ predicted by PA- or PI-related variables do not track observed $\Delta BC/\Delta CO$ as well as PF-predicted $\Delta BC/\Delta CO$.~~ These results suggest that ~~PF~~ PI (and to a lesser degree PF) ~~may be more important than~~ must be accounted for when ~~PA and PI for~~ predicting aerosol scavenging over the tropical West Pacific. This further implies that even though precipitation may be occurring, it may not be efficiently scavenging aerosol.

Comparing which precipitation products among the top predictors (by R), most good-performing precipitation-based predictors used SPP-based precipitation such as IMERG or PERSIANN-CDR (Fig. 2c-e). ~~Noticeably, only one precipitation-related predictor calculated from GFS met the R threshold ($PI_{PCP > 0.mm2, 72H, GFS}$; Fig. 2b).~~ This suggests that GFS-derived precipitation variables are not as able to capture observed TE_{BC} ~~$\Delta BC/\Delta CO$~~ trends ~~in contrast to several SPP-based precipitation variables that showed moderate to strong R (> 0.71) with $\Delta BC/\Delta CO$~~. The poor performance of GFS-derived precipitation is reflective of past studies showing disagreements in precipitation characteristics between satellite and reanalyses (Cannon et al., 2017; Jiang et al., 2021) and even divergent precipitation trends and amounts among individual reanalysis products (Alexander et al., 2020; Chen et al., 2020b; Barrett et al., 2020). Our results ~~suggest~~ corroborates previous work that precipitation from GFS reanalysis is not a reliable predictor of aerosol scavenging compared to precipitation from SPPs. Future studies relating precipitation to aerosol scavenging are recommended to instead rely on in situ or satellite retrieved precipitation rather than precipitation from reanalysis.

Predictors based on ~~quantiles~~ quantiles of RH (e.g., RH_{q90}) (Fig. 2b) perform quite well, with high ~~based on~~ R and ~~,~~ slope (Fig. 2e) and ~~,~~ intercept ~~,~~ and WAD consistently close to 0 regardless of quantile (Fig. 3~~2~~b~~e~~). RH_{q90} performs slightly better in terms of R than other RH thresholds (Fig. 2b~~e~~); however, this difference is minor as shown by the overlapping 25^{th}-75^{th} percentile error bars between the different RH ~~thresholds~~ quantiles. The similar performance between different RH quantiles suggests consistency in their ability to predict TE_{BC}~~$\Delta BC/\Delta CO$~~ trends (high R; Fig. 2b) while doing reasonably better than other types of predictors when

Formatted: Not Superscript/ Subscript
Formatted: Subscript
Formatted: Subscript
Formatted: Subscript
Formatted: Subscript
Formatted: Subscript
Formatted: Subscript

estimating TE_{BC} ~~ΔBC/ΔCO~~ magnitudes across the spectrum of predictor values (intercepts closer to 0, slopes closer to 1). Maximum RH along trajectories was used by Kanaya et al. (2016) in their analysis of ΔBC/ΔCO scavenging to detect the role of clouds in BC removal. Our findings suggest that top quantiles of RH, including its maximum, are ~~a~~ good choices for ~~predicting scavenging~~estimating TE_{BC} ~~trends~~.

Formatted: Subscript

Compared to variables directly linked to precipitation (PA, PF, PI, APT), the slopes from RH quantiles are noticeably closer to the ideal value of 1 (Fig. 2b~~e~~) while their intercepts ~~from RH quantiles~~ are closer to the ideal value of 0 (Fig. 2b~~e~~), meaning TE_{BC}~~ΔBC/ΔCO~~ predicted by RH quantiles more closely matches the ~~magnitude of~~ observed TE_{BC} ~~ΔBC/ΔCO compared to~~ than TE_{BC} ~~ΔBC/ΔCO~~ predicted by precipitation. We hypothesize that the better performance of RH-related predictors over those more directly related to precipitation (e.g., APT) may be explained by instances of precipitation that ~~is~~ are missed (or misestimated) by SPP retrievals that ~~is~~ are indirectly detected by reanalysis as high humidity conditions. This possibility is supported by previous literature showing the tendency of SPPs to misestimate light (Nadeem et al., 2022; Kidd et al., 2021) or intense precipitation (Chen et al., 2020a; Gupta et al., 2020); however, we cannot rule out the possibility of the hygroscopic growth~~(Kanaya et al., 2016)~~, in-cloud activation (high RH), and subsequent removal of BC during transport. Thus, our hypothesis of ~~the connection between~~ RH from reanalysis ~~and~~ capturing missed precipitation from SPPs requires further investigation in future work.

Of all the fractional predictors considered in this study, f_{MR15} and f_{RH95} perform the best (Fig. 2b~~d~~). f_{MR15} and f_{RH95} reflect the frequency of occurrence of scavenging-conducive conditions during transport. A high frequency of high MR or RH may indicate that air masses passed through large areas of clouds and/or precipitation during long-range transport. ~~Interestingly,~~f_{RH95} has a median slope of 0.99 (Fig. 2b), a ~~the~~ 25th-75th percentile range in slope of ~~slopes from f_{RH95} (~~0.~~81~~92 – 1.02~~20~~ (Fig. 2b)~~; Fig. 2d),~~ and~~-~~ a median intercept of 0.01 ~~overlaps with the ideal value of 1 and its intercepts ((~0.25;~~ Fig. 3~~2~~b~~d~~) ~~are lower than the other predictors in Fig. ,2. These slope and intercept statistics~~ indicating that ~~e that f_{RH95} is capable estimating the magnitude of ΔBC/ΔCO throughout the spectrum of f_{RH95} values, meaning that~~ f_{RH95} can be used to capture TE_{BC}~~ΔBC/ΔCO~~ trends and magnitudes ~~for~~ for a wide range of TE_{BC}~~both high-ΔBC/ΔCO (fresh) and low-ΔBC/ΔCO (scavenged) air masses~~. ~~A similar performance is observed for f_{MR15}. f_{MR15} and f_{RH95} are similar to PF, which was the best-performing category of precipitation-related predictors, in that PF, f_{MR15}, and f_{RH95} represent the occurrence frequencies of some condition along each trajectory (e.g., non-zero precipitation or RH > 95%).~~ The ~~better~~ good performance of f_{MR15} and f_{RH95} ~~these frequency-related predictors compared to other types of predictors~~ suggests that the frequency ~~of precipitation or high-RH~~ of scavenging-conducive conditions may be more reliable indicators of aerosol scavenging than ~~the magnitude of~~ precipitation amount (e.g., APT, ~~PI,~~ PA).

~~One limitation of our analysis is the goodness-of-fit achieved during the k-fold cross-validation process as the goodness-of-fit affects the validity of interpreting the resulting performance statistics (e.g., slope). Fig. S1 of the Supplementary Information (SI) shows no large difference in the goodness-of-fit between different predictors based on R and RMSE. Similar magnitudes of RMSE (Fig. S1) suggest that the interpretation of performance statistics derived from the curve-fitting procedure is equally valid across the discussed predictors.~~

3.2 Nonlinear sensitivity of TE_{BC}~~ΔBC/ΔCO~~ to meteorological variables

Although the predictors in Figs. 2 – 3 exhibit the highest R of all predictors considered in this study, their slopes are generally below 1 (Fig. 2) while their intercepts and WAD are generally positive (Fig. 3). The combination of these statistics implies that predictions of TE_{BC} ~~ΔBC/ΔCO~~ using our method tend to overestimate observed TE_{BC} ~~ΔBC/ΔCO~~ across the spectrum of predictor values (indicated by WAD > 0) with maximum overestimations occurring when observed TE_{BC} ~~ΔBC/ΔCO~~ is low (indicated by slopes < 1 and intercepts > 0). This points to a nonlinear sensitivity of TE_{BC} ~~ΔBC/ΔCO~~ to these predictors as the degree of scavenging increases. Dadashazar et al. (2021) observed a similar nonlinear response to APT by a ratio of particulate matter below

2.5 µm to CO ($\Delta PM_{2.5}/\Delta CO$), where $\Delta PM_{2.5}/\Delta CO$ was most responsive to APT when APT was below 5 mm and less sensitive to APT when APT exceeded 5 mm.

Investigating this sensitivity further, Fig. 4 shows that PF-predicted TE_{BC} ~~ΔBC/ΔCO~~ does not capture the trends of observed TE_{BC} ~~ΔBC/ΔCO~~ for highly scavenged air masses. In other words, PF loses its predictive power as the degree of scavenging increases, implying that PF is most important for the scavenging of fresher air masses (high-TE_{BC}~~ΔBC/ΔCO~~). This nonlinear sensitivity of TE_{BC} ~~ΔBC/ΔCO~~ ~~t~~to~~o~~ PF hints at the possibility that other meteorological variables may become important for further scavenging of highly scavenged air (low-TE_{BC}~~ΔBC/ΔCO~~). In contrast to predictors directly related to precipitation (Fig. 4d-f), the predicted curves of RH_{q95} (Fig. 4a), f_{RH95} (Fig. 4b), and f_{MR15} (Fig. 4c) visibly track the trends of observed TE_{BC}~~ΔBC/ΔCO~~ with approximately half the difference between predicted and observed TE_{BC} ~~ΔBC/ΔCO~~ when TE_{BC} ~~ΔBC/ΔCO~~ is low. The capability of RH_{q95}, f_{RH95}, and f_{MR15} to predict TE_{BC} ~~ΔBC/ΔCO~~ across a wider range of values is further reflected by generally lower intercepts and WAD (Fig. 3) than precipitation-related predictors, which suggests promising alternative indicators of aerosol scavenging. However, we also note that such differences could arise partly from the limitations of curve-fitting, wherein fitted curves naturally capture gradual changes (e.g., Fig. 4b) better than sharp ones (e.g., Fig. 4d).

3.3 ~~Effect of filtering APT on performance~~Applying filters to improve the predictive power of precipitation-related variables

In this section, we examine the predictive power of precipitation-related variables when applying the following filters:~~To improve the predictive performance of precipitation-related variables, we applied combinations of filters for~~ (1) precipitation intensity, (2) trajectory altitude, (3) data product, and (4) trajectory length, with ~~.~~the objective to identify what factors are important when relating precipitation along trajectories to TE_{BC}. Filtering for precipitation intensity isolates the contribution of higher precipitation intensities towards a precipitation-related predictor's ability to predict TE_{BC}~~ΔBC/ΔCO~~. Intense precipitation has been shown to be more efficient at scavenging aerosol particles (Zhao et al., 2020) and may be important when estimating aerosol scavenging. Filtering for trajectory altitude (i.e., considering precipitation only when the trajectory altitude is below 1.5 km AGL) tests the hypothesis that air masses within the boundary layer will be most susceptible to wet scavenging. Grythe et al. (2017) demonstrated that below-cloud scavenging (i.e., impaction by precipitation) accounted for majority of scavenging events below 1 km. We selected 1.5 km based on previous work on the marine boundary layer over the tropical West Pacific (Chien et al., 2019). We repeated the analysis for three precipitation products (one reanalysis and two SPPs) to capture variability in our results due to the choice of data product which has been shown to be important for precipitation (Alexander et al., 2020). Finally, we tested the effect of trajectory length on the performance of APT as a predictor of TE_{BC}~~ΔBC/ΔCO~~. We performed these sensitivity tests on APT (Fig. 5), PI (Fig. S4), PF (Fig. S5), and PA (Fig. S6).

In general, we found that applying altitude and/or precipitation filters negatively affected the performance of APT (Fig. 5b-d), PF (Fig. S5b-d, except for PERSIANN-CDR), and PA (Fig. S6b-d)~~,~~, leading to lower R between predicted and observed TE_{BC} ~~ΔBC/ΔCO~~ compared to ~~the case~~ the case without any filters ~~applied~~ (Fig. 5a). Two exceptions were: PF from PERSIANN-CDR (colored yellow in Fig. S5), which could be used to estimate TE_{BC} if we applied both an altitude filter (< 1500 m) and a precipitation intensity filter (> 0.2 mm h^{-1}) over longer back trajectory times (> 48 hours) (Fig. S5d), and PI, which could be used to estimate TE_{BC} when filtering for precipitation intensities (> 0.2 mm h^{-1}) and along trajectories longer than 48 hours (Fig. S4b). The better performance of PI across multiple SPPs (Fig. S4) is an encouraging sign that this improvement is robust and points to the contribution of higher precipitation intensities towards total scavenging.~~The poorer performance of precipitation filtered for higher intensities (Fig. 5b) suggests that these higher intensities may not be as important for estimating wet scavenging compared to low intensity precipitation, consistent with previous work showing that light rain exerts more control over the global aerosol burden~~

Formatted: Subscript

Formatted: Subscript

Formatted: Superscript

Formatted: Subscript

Formatted: Not Superscript/ Subscript

Formatted: Superscript

~~(Wang et al., 2021b) and that precipitation over the tropical West Pacific is typically high in frequency and low to moderate in intensity (Biasutti et al., 2012).~~

Applying a filter for trajectory altitude prior to calculating APT also did not lead to large improvements in R (Fig. 5c). This was surprising because, when using total column precipitation from SPPs, a maximum altitude filter should reduce errors from cases where precipitation occurs below the air mass and no scavenging occurs. Since the SPPs used in this study have been validated using surface measurements (Sapiano and Arkin, 2009; Nicholson et al., 2019; Wang et al., 2021a), precipitation from SPPs should be reflective of precipitation that reaches the surface, implying a susceptibility of these SPPs to errors related to virga (Wang et al., 2018). However, Wang et al. (2018) also showed that virga occurrence over the tropical West Pacific is also infrequent. An alternative explanation for the poor performance of altitude-filtered ~~predictors~~ APT is uncertainties related to trajectory altitude (Harris et al., 2005), such that an air parcel may have actually been traveling at a lower altitude than its modelled trajectory and underwent more scavenging than predicted using APT.

An examination of trajectory altitudes (Fig. S7~~5~~) revealed that filtering for trajectory altitudes below 1.5 km excluded the majority (~70%) of precipitating grid cells encountered by trajectories, which likely negatively impacted the predictive ability of altitude-filtered predictors.

Longer trajectories resulted in slightly higher R between observed and ~~APT-predicted~~ predicted TE_{BC} using APT from PERSIANN-CDR or IMERG ~~ΔBC/ΔCO~~ (Fig. 5a-b)~~, increasing from R ~0.5 to ~0.6~~; however, this difference is not large, as shown by overlapping 25th-75th percentile error bars. Interestingly, this increase in R for longer trajectories was more evident when filtering for precipitation intensities > 0.2 mm h^{-1} when calculating APT (Fig. 5b) or PI (Fig. ~~S2b~~S4b), but not when applying this intensity filter on PF (Fig. S3b) or PA (Fig. S4b). Further interpretation likely requires a physical model in future work to explain why the performance of intense precipitation (Fig. 5b) benefits from a longer trajectory more than total precipitation does (Fig. 5a).

4 Limitations

TE_{BC} ~~ΔBC/ΔCO~~ as a wet scavenging proxy: In this study, we treat TE_{BC} ~~ΔBC/ΔCO~~ as a proxy for wet scavenging (i.e., predictand) and base our conclusions on which variables (i.e., predictors) best predict TE_{BC}~~this ratio (i.e., predictors)~~. ~~An underlying assumption is that there is negligible emission of BC or CO after initial emission and after wet scavenging occurs.~~ Dilution or entrainment during transport is expected to influence the ΔBC/ΔCO ratio and therefore TE_{BC}. While the use of the CAMS-GLOB-ANT emission inventory (Sect. 2.4) when calculating $ER_{BC/CO}$ (Sect. 2.5) reduces this uncertainty by accounting for potential surface influence during transport close to the surface, the resolutions of both the trajectory meteorological input (0.25 × ~~x~~ 0.25°) and the emission inventory (0.1 × ~~x~~ 0.1°) remain limiting factors. Thus, our analysis assumes that wet scavenging is the main driver of changes in TE_{BC} and chemical transport modelling in future work is needed to quantify the effect of mixing on TE_{BC}. Consequently, this method is expected to work well in outflow regions such as the tropical West Pacific and not well where additional BC and/or CO are likely to be after initial emission or wet scavenging has occurred (e.g., continental region).

~~**ΔBC/ΔCO depends on air mass type**: The ΔBC/ΔCO quantity is also affected by air mass type. For example, biomass burning and anthropogenic/industrial emissions will have different ΔBC/ΔCO values (e.g., Hilario et al., 2021). The mixing state and composition of BC-containing particles will also affect its hygroscopicity and by extension its rate of wet scavenging (Liu et al., 2013). Although these factors are expected to influence ΔBC/ΔCO, we assume the response of ΔBC/ΔCO to the predictor will be chiefly determined by scavenging-related processes. While the response of ΔBC/ΔCO to APT in Hilario et al. (2021) was quite similar across different air mass origins (their Fig. 9), this may not be always the case. However, this origin-independent~~

Formatted: Font: Bold

Formatted: Subscript

~~relationship does allow for the option of curve-fitting without differentiating between individual sources. Beneficially, this choice to aggregate the data rather than resolving by source increases the number of data points available for curve-fitting, which improves the robustness of the resulting statistics and adds strength to our conclusions on which meteorological variables are most relevant for aerosol scavenging.~~

~~Specific processes~~Method does not discriminate between in- or below-cloud scavenging:~~:~~ The conclusions of our study are based on the relative ability of different variables to predict TE_{BC}~~$\Delta BC/\Delta CO$~~, our proxy for wet scavenging. This approach does not isolate individual processes that are usually parameterized by global circulation models (e.g., impaction, nucleation) (Croft et al., 2009, 2010; Ryu and Min, 2022) and does not discriminate between in-cloud or below-cloud scavenging. However, through our proposed framework, we can still gain qualitative insights into which meteorological variables are relevant for estimating aerosol scavenging, which can inform future studies as well as developments in model parametrization.

Single predictor method: The method presented here assesses the one-to-one relationship between a single predictor and TE_{BC} ~~$\Delta BC/\Delta CO$~~ repeated individually for several predictors. We expect that using a combination of predictors may lead to better predictions of TE_{BC} ~~$\Delta BC/\Delta CO$~~ while providing a more physical picture of relative contributions of different meteorological variables towards wet scavenging. Future work may utilize multiple linear regression or more sophisticated methods such as machine learning to consider different combinations of predictors with the objective of identifying a combination that predicts TE_{BC} ~~$\Delta BC/\Delta CO$~~ well and extracting further information on what physical mechanisms may be relevant for the removal of TE_{BC} ~~$\Delta BC/\Delta CO$~~ based on relative coefficients or weightings of different predictors.

Curve-fitting: The results can depend on the curve-fitting function used. Different variables are expected to have different relationships with ~~$\Delta BC/\Delta CO$~~TE_{BC}. Thus, ~~if we~~ consider~~ed~~ing only one function for curve-fitting~~, it would~~ favors variables that have a specific relationship with TE_{BC}~~$\Delta BC/\Delta CO$~~. To reduce this bias, we applied four different curve-fitting functions (Table 2) on each predictor based on two equations from previous studies (Kanaya et al., 2016; Oshima et al., 2012) and two equations of generalized form ~~(Table 2)~~ that accounted for possible relationships between TE_{BC}~~$\Delta BC/\Delta CO$~~ and each predictor. We then chose the curve-fitting function that produced the highest R between observed and predicted TE_{BC}~~$\Delta BC/\Delta CO$~~. However, we note that this does not completely remove the bias as specific functions were still selected.

Trajectory modeling: Vertical motion through convection, entrainment, and detrainment processes are known uncertainties in trajectory modeling, which increase with trajectory length (Harris et al., 2005). The spatial and temporal resolutions of the meteorological input used for the HYSPLIT model are also limiting factors as meteorology along HYSPLIT trajectories do not account for sub-timestep or sub-grid processes.

5 Conclusions

We present a method to identify meteorological indicators of aerosol scavenging using a combination of aircraft, satellite, and reanalysis data coupled with HYSPLIT backward trajectories. We apply this method to the CAMP^{2}Ex field campaign over the tropical West Pacific, which hosts a wide range of cloud fractions and precipitation characteristics as well as an environment characterized by long-range transport of aerosol and trace gas species. ~~Since $\Delta BC/\Delta CO$ is mainly affected by scavenging, we treat $\Delta BC/\Delta CO$ as an in situ proxy for aerosol scavenging and~~ We evaluate ~~the responses of~~ which meteorological variables can be used to predict TE_{BC}~~$\Delta BC/\Delta CO$~~ ~~to different meteorological variables~~ (i.e., predictors). The main conclusions of the study are the following:

Formatted: Not Superscript/ Subscript

Formatted: Subscript

1. Although APT has been utilized in several studies as an indicator of aerosol scavenging, we demonstrate~~d~~ that APT does poorly when -predicting~~ed~~ TE_{BC} ~~$\Delta BC/\Delta CO$ (e.g., does not track observed $\Delta BC/\Delta CO$ well~~weak correlations, underestimates TE_{BC}). Furthermore, the application of altitude or precipitation intensity filters negatively impact~~ed~~ the performance of APT in predicting TE_{BC}~~$\Delta BC/\Delta CO$ trends~~. Since APT is an accumulated precipitation amount over the whole trajectory, APT does not account for other precipitation characteristics such as intensity or frequency, which have been shown to be relevant for aerosol scavenging. This shortcoming may explain the overall poor relative performance of APT in predicting TE_{BC}~~$\Delta BC/\Delta CO$~~.

~~2. To investigate which precipitation characteristics are most relevant for predicting aerosol scavenging, we calculated PA, PF, and PI along trajectories using precipitation from reanalysis (GFS) and SPPs (IMERG, PERSIANN-CDR). While several precipitation-related predictors calculated from SPPs were able to predict $\Delta BC/\Delta CO$ reasonably well, only one precipitation-related predictor from GFS correlated with $\Delta BC/\Delta CO$ ($R > 0.71$), suggesting that precipitation from SPPs may be better at predicting aerosol scavenging than precipitation from reanalysis. The poorer performance of precipitation from reanalysis in predicting $\Delta BC/\Delta CO$ than from SPPs is corroborated by previous studies that found larger misestimates of precipitation by reanalysis than by SPPs. Because of our results and those of past studies, we recommend relying on in situ or SPP precipitation rather than precipitation from reanalysis, particularly when relating precipitation to aerosol scavenging.~~

~~3. Frequency-related predictors such as PF, f_{MR15}, and f_{RH95} performed much better than APT in predicting $\Delta BC/\Delta CO$ trends and magnitudes. PF, f_{MR15}, and f_{RH95} represent the frequencies of occurrence of some meteorological condition along trajectories such as non-zero precipitation (PF) or RH exceeding 95% (f_{RH95}). The relatively better performance of these frequency-related predictors over those related to PA or PI suggests that the frequency of precipitation or high-RH conditions may be a more reliable indicator of aerosol scavenging than the magnitude of precipitation.~~

2. Predictors based on specific quantiles ~~or the mean~~ of RH (e.g., RH_{90}) also perform~~ed~~ quite well in predicting both TE_{BC} ~~$\Delta BC/\Delta CO$~~ trends and magnitudes (intercepts close to zero, WAD close to zero, slopes close to 1, R close to 1). We ~~found~~ find only minor differences in the performance depending on the exact quantile used, suggesting the RH distribution during transport is a robust way to estimate TE_{BC}. We hypothesize the outperformance of RH quantiles over predictors more directly related to precipitation (e.g., APT) to be due to missed precipitation in SPP retrievals that was indirectly represented in reanalysis as high humidity conditions~~. Such a possibility is supported by previous literature demonstrating that SPPs tend to misestimate light precipitation (Nadeem et al., 2022; Kidd et al., 2021)~~; however, further work is required to explore this ~~hypothesis~~possibility.

3. Frequency-related predictors such as f_{MR15} and f_{RH95} perform~~ed~~ better than APT in predicting TE_{BC} trends (higher R) and magnitudes (slopes closer to 1). f_{MR15}~~,~~ and f_{RH95} represent the frequencies along 72-h trajectories of MR exceeding 15 g kg^{-1} and RH exceeding 95%, respectively. The abilities of f_{MR15} and f_{RH95} to predict TE_{BC} suggests that the frequency of humid conditions should be considered when estimating aerosol scavenging.

4. To investigate which precipitation characteristics are most relevant for predicting TE_{BC}, we quantif~~ied~~y PA, PF, and PI along trajectories and f~~ou~~ind that PI ~~wa~~is the most effective at estimating TE_{BC} when we calculate~~d~~ PI over longer trajectories (> 48 h) and only includ~~ing~~e grid cells with precipitation > 0.2 mm h^{-1} in our calculation. This points to the contribution of intense precipitation and the importance of accounting for air mass history when estimating aerosol scavenging.

~~4.~~5. We f~~ou~~ind that precipitation from SPPs (IMERG, PERSIANN-CDR) is generally better at predicting TE_{BC} (higher R) than precipitation from reanalysis (GFS). This is corroborated by previous studies that found larger misestimates of

Formatted: Subscript

Formatted: Subscript

Formatted: Subscript

Formatted: Superscript

Formatted: Subscript

Formatted: Subscript

Formatted: Subscript

Formatted: Superscript

precipitation by reanalysis than by SPPs. Because of our results and those of past studies, we recommend relying on in situ or SPP precipitation rather than precipitation from reanalysis, particularly when relating precipitation to aerosol scavenging.

Given these findings, we recommend the following alternatives to APT when estimating aerosol scavenging: (1) RH quantiles (e.g., 90th percentile of RH along trajectories), (2) f_{MR15} or f_{RH95}, and (3) PI from SPPs filtered for grid cells with precipitation > 0.2 mm h^{-1}. These variables were found to be able to predict TE_{BC} more accurately than APT; thus, future scavenging parametrizations should consider these meteorological variables along air mass histories.

~~By identifying which meteorological variables are relevant for predicting ΔBC/ΔCO trends (and by extension, aerosol wet scavenging), the findings of this study may be useful for informing future aerosol scavenging studies. Furthermore, these results may also aid in improving scavenging parametrization schemes in models.~~ Future work is encouraged to ~~The method presented in this study is repeatable~~ apply this method over a variety of environments (e.g., using other data from other field campaigns), ~~and is relatively computationally inexpensive to apply. Future work may~~ utilize machine learning to ~~identify~~ assess what combinations of meteorological variables are relevant for ~~to~~ predicting aerosol scavenging, and apply ~~our~~ this method to ~~different~~ other regions to ~~identify~~ determine if there are region~~-specific~~al differences in indicators of aerosol scavenging. Furthermore, CAMP^{2}Ex included a rich dataset on cloud water composition (Crosbie et al., 2022; Stahl et al., 2021) that can be explored, as in past work for other regions (MacDonald et al., 2018), to gain additional insights into aerosol wet scavenging processes.

Appendix A: Describing the transport of BC and CO during CAMP^{2}Ex

During the CAMP^{2}Ex field campaign, BC and CO originated from several sources. Long-range transport patterns during the campaign and associated air mass composition are described in ~~(~~Hilario et al. (~~,~~2021) but here we present a summary of their findings related to the transport of BC and CO. The CAMP^{2}Ex field campaign

overlapped with the end of the southwest monsoon and the beginning of the monsoon transition (Reid et al., 2023). Because of this, a synoptic shift occurred during the campaign (~~(~~Hilario et al., 2021; ~~)~~ their Figs. 2-3) that allowed for the sampling of transported air masses from different source regions such as East Asia and the Maritime Continent. Hilario et al. (2021) identified four major source regions for long-range transport: East Asia (e.g., China, Korea), the Maritime Continent (e.g., Indonesia, Malaysia), Peninsular Southeast Asia (e.g., Vietnam), and the West Pacific (i.e., ocean). The presence of long-range transport was detected throughout the whole campaign (their Fig. S2).

The Maritime Continent during the campaign was undergoing its burning season which is well-established in the literature to lead to high aerosol loadings that can be transported over large distances (Xian et al., 2013). Hilario et al. (2021) showed that air masses from the Maritime Continent and East Asia were transported under relatively dry conditions, which in this study manifested as higher ΔBC/ΔCO (Fig. S1a) and TE_{BC} (Fig. S1d), and were associated with southwesterly monsoon flow and the passage of typhoons, respectively. These conditions were conducive for long-range transport and led to the sampling of higher concentrations of BC and CO in air from East Asia (BC: 87.29 ng m^{-3}; CO: 0.16 ppm) and the Maritime Continent (BC: 71.81 ng m^{-3}; CO: 0.18 ppm) than in air from Peninsular Southeast Asia (BC: 24.90 ng m^{-3}; CO: 0.10 ppm) or the West Pacific (BC: 1.03 ng m^{-3}; CO: 0.08 ppm). We note that Hilario et al. (2021) kept CO in units of ppm while we converted CO to mass concentration units such that ΔBC/ΔCO would be unitless. Hilario et al. (2021) demonstrated that the scavenging of air from Peninsular Southeast Asia was related to convective lofting as air from Peninsular Southeast Asia sampled in the free troposphere (> 1.5 km) had much lower aerosol concentrations than air from the region sampled in the boundary layer (< 1.5 km) (their Fig. S6). These findings point to the active role of scavenging in determining aerosol loadings in transported air masses during CAMP^{2}Ex.

Formatted: Normal, No bullets or numbering
Formatted: Superscript
Formatted: Subscript
Formatted: Subscript
Formatted: Superscript
Formatted: Subscript
Formatted: Superscript
Formatted: Heading 1
Formatted: Superscript
Formatted: Indent: First line: 0.5"
Formatted: Superscript
Formatted: Subscript
Formatted: Superscript
Formatted: Superscript

Code availability. Codes are freely available upon request to the authors.

Data availability. All datasets are publicly available and accessible at https://doi.org/10.5067/Suborbital/CAMP2EX2018/DATA001 (NASA/LaRC/SD/ASDC, 2020). HYSPLIT data are accessible through the NOAA READY website (https://www.ready.noaa.gov/index.php, last access: 11 April 2023) (NOAA Physical Sciences Laboratory, 2020).

Author contributions. EC, LDZ, MAS, JPD, GSD contributed to data collection. MRAH and AS conceptualized the study. MRAH performed the data analysis and prepared the manuscript with input from all co-authors.

Competing interests. The authors declare that they have no conflict of interest.

Disclaimer. Publisher's note: Copernicus Publications remains neutral with regard to jurisdictional claims in published maps and institutional affiliations.

Special issue statement. This article is part of the special issue "Cloud Aerosol and Monsoon Processes Philippines Experiment (CAMP^{2}Ex) (ACP/AMT inter-journal SI)". It is not associated with a conference.

Acknowledgements. This research has been supported by the National Aeronautics and Space Administration (grant no. 80NSSC18K0148).

6 References

Alexander, L. V., Bador, M., Roca, R., Contractor, S., Donat, M. G., and Nguyen, P. L.: Intercomparison of annual precipitation indices and extremes over global land areas from in situ, space-based and reanalysis products, Environ. Res. Lett., 15, 055002, https://doi.org/10.1088/1748-9326/ab79e2, 2020.

Andronache, C.: Estimated variability of below-cloud aerosol removal by rainfall for observed aerosol size distributions, Atmospheric Chemistry and Physics, 3, 131–143, https://doi.org/10.5194/acp-3-131-2003, 2003.

NOAA Physical Sciences Laboratory: https://psl.noaa.gov/data/gridded/index.html, last access: 13 June 2020.

Ashouri, H., Hsu, K.-L., Sorooshian, S., Braithwaite, D. K., Knapp, K. R., Cecil, L. D., Nelson, B. R., and Prat, O. P.: PERSIANN-CDR: Daily Precipitation Climate Data Record from Multisatellite Observations for Hydrological and Climate Studies, Bull. Amer. Meteor. Soc., 96, 69–83, https://doi.org/10.1175/BAMS-D-13-00068.1, 2015.

Barrett, A. P., Stroeve, J. C., and Serreze, M. C.: Arctic Ocean Precipitation From Atmospheric Reanalyses and Comparisons With North Pole Drifting Station Records, Journal of Geophysical Research: Oceans, 125, e2019JC015415, https://doi.org/10.1029/2019JC015415, 2020.

Bellouin, N., Quaas, J., Gryspeerdt, E., Kinne, S., Stier, P., Watson-Parris, D., Boucher, O., Carslaw, K. S., Christensen, M., Daniau, A.-L., Dufresne, J.-L., Feingold, G., Fiedler, S., Forster, P., Gettelman, A., Haywood, J. M., Lohmann, U., Malavelle, F., Mauritsen, T., McCoy, D. T., Myhre, G., Mülmenstädt, J., Neubauer, D., Possner, A., Rugenstein, M., Sato, Y., Schulz, M., Schwartz, S. E., Sourdeval, O., Storelvmo, T., Toll, V., Winker, D., and Stevens, B.: Bounding Global Aerosol Radiative Forcing of Climate Change, Reviews of Geophysics, 58, e2019RG000660, https://doi.org/10.1029/2019RG000660, 2020.

Biasutti, M., Yuter, S. E., Burleyson, C. D., and Sobel, A. H.: Very high resolution rainfall patterns measured by TRMM precipitation radar: seasonal and diurnal cycles, Clim Dyn, 39, 239–258, https://doi.org/10.1007/s00382-011-1146-6, 2012.

Breiman, L. and Spector, P.: Submodel Selection and Evaluation in Regression. The X-Random Case, International Statistical Review / Revue Internationale de Statistique, 60, 291–319, https://doi.org/10.2307/1403680, 1992.

Cannon, F., Ralph, F. M., Wilson, A. M., and Lettenmaier, D. P.: GPM Satellite Radar Measurements of Precipitation and Freezing Level in Atmospheric Rivers: Comparison With Ground-Based Radars and Reanalyses, Journal of Geophysical Research: Atmospheres, 122, 12,747-12,764, https://doi.org/10.1002/2017JD027355, 2017.

Chen, H., Yong, B., Qi, W., Wu, H., Ren, L., and Hong, Y.: Investigating the Evaluation Uncertainty for Satellite Precipitation Estimates Based on Two Different Ground Precipitation Observation Products, Journal of Hydrometeorology, 21, 2595–2606, https://doi.org/10.1175/JHM-D-20-0103.1, 2020a.

Chen, S., Liu, B., Tan, X., and Wu, Y.: Inter-comparison of spatiotemporal features of precipitation extremes within six daily precipitation products, Clim Dyn, 54, 1057–1076, https://doi.org/10.1007/s00382-019-05045-z, 2020b.

Chien, F.-C., Hong, J.-S., and Kuo, Y.-H.: The Marine Boundary Layer Height over the Western North Pacific Based on GPS Radio Occultation, Island Soundings, and Numerical Models, Sensors, 19, 155, https://doi.org/10.3390/s19010155, 2019.

Choi, Y., Kanaya, Y., Takigawa, M., Zhu, C., Park, S.-M., Matsuki, A., Sadanaga, Y., Kim, S.-W., Pan, X., and Pisso, I.: Investigation of the wet removal rate of black carbon in East Asia: validation of a below- and in-cloud wet removal scheme in FLEXible PARTicle (FLEXPART) model v10.4, Atmospheric Chemistry and Physics, 20, 13655–13670, https://doi.org/10.5194/acp-20-13655-2020, 2020.

Coelho, L. P.: Jug: Software for Parallel Reproducible Computation in Python, 5, 30, https://doi.org/10.5334/jors.161, 2017.

Crippa, M., Guizzardi, D., Muntean, M., Schaaf, E., Dentener, F., van Aardenne, J. A., Monni, S., Doering, U., Olivier, J. G. J., Pagliari, V., and Janssens-Maenhout, G.: Gridded emissions of air pollutants for the period 1970–2012 within EDGAR v4.3.2, Earth System Science Data, 10, 1987–2013, https://doi.org/10.5194/essd-10-1987-2018, 2018.

Croft, B., Lohmann, U., Martin, R. V., Stier, P., Wurzler, S., Feichter, J., Posselt, R., and Ferrachat, S.: Aerosol size-dependent below-cloud scavenging by rain and snow in the ECHAM5-HAM, Atmos. Chem. Phys., 23, 2009.

Croft, B., Lohmann, U., Martin, R. V., Stier, P., Wurzler, S., Feichter, J., Hoose, C., Heikkila, U., van Donkelaar, A., and Ferrachat, S.: Influences of in-cloud aerosol scavenging parameterizations on aerosol concentrations and wet deposition in ECHAM5-HAM, Atmos. Chem. Phys., 33, 2010.

Crosbie, E., Ziemba, L. D., Shook, M. A., Robinson, C. E., Winstead, E. L., Thornhill, K. L., Braun, R. A., MacDonald, A. B., Stahl, C., Sorooshian, A., van den Heever, S. C., DiGangi, J. P., Diskin, G. S., Woods, S., Bañaga, P., Brown, M. D., Gallo, F., Hilario, M. R. A., Jordan, C. E., Leung, G. R., Moore, R. H., Sanchez, K. J., Shingler, T. J., and Wiggins, E. B.: Measurement report: Closure analysis of aerosol–cloud composition in tropical maritime warm convection, Atmospheric Chemistry and Physics, 22, 13269–13302, https://doi.org/10.5194/acp-22-13269-2022, 2022.

Dadashazar, H., Alipanah, M., Hilario, M. R. A., Crosbie, E., Kirschler, S., Liu, H., Moore, R. H., Peters, A. J., Scarino, A. J., Shook, M., Thornhill, K. L., Voigt, C., Wang, H., Winstead, E., Zhang, B., Ziemba, L., and Sorooshian, A.: Aerosol responses to precipitation along North American air trajectories arriving at Bermuda, Atmospheric Chemistry and Physics, 21, 16121–16141, https://doi.org/10.5194/acp-21-16121-2021, 2021.

Feng, J.: A 3-mode parameterization of below-cloud scavenging of aerosols for use in atmospheric dispersion models, Atmospheric Environment, 41, 6808–6822, https://doi.org/10.1016/j.atmosenv.2007.04.046, 2007.

Flossmann, A. I., Hall, W. D., and Pruppacher, H. R.: A Theoretical Study of the Wet Removal of Atmospheric Pollutants. Part I: The Redistribution of Aerosol Particles Captured through Nucleation and Impaction Scavenging by Growing Cloud Drops, Journal of the Atmospheric Sciences, 42, 583–606, https://doi.org/10.1175/1520-0469(1985)042<0583:ATSOTW>2.0.CO;2, 1985.

Frey, L., Bender, F. A.-M., and Svensson, G.: Processes controlling the vertical aerosol distribution in marine stratocumulus regions – a sensitivity study using the climate model NorESM1-M, Atmospheric Chemistry and Physics, 21, 577–595, https://doi.org/10.5194/acp-21-577-2021, 2021.

Ge, C., Wang, J., and Reid, J. S.: Mesoscale modeling of smoke transport over the Southeast Asian Maritime Continent: coupling of smoke direct radiative effect below and above the low-level clouds, Atmos. Chem. Phys., 14, 159–174, https://doi.org/10.5194/acp-14-159-2014, 2014.

Granier, C., Darras, S., Denier van der Gon, H., Doubalova, J., Elguindi, N., Galle, B., Gauss, M., Guevara, M., Jalkanen, J.-P., Kuenen, J., Liousse, C., Quack, B., Simpson, D., and Sindelarova, K.: The Copernicus Atmosphere Monitoring Service global and regional emissions (April 2019 version), https://doi.org/10.24380/D0BN-KX16, 2019.

Grythe, H., Kristiansen, N. I., Groot Zwaaftink, C. D., Eckhardt, S., Ström, J., Tunved, P., Krejci, R., and Stohl, A.: A new aerosol wet removal scheme for the Lagrangian particle model FLEXPART v10, Geoscientific Model Development, 10, 1447–1466, https://doi.org/10.5194/gmd-10-1447-2017, 2017.

Gupta, V., Jain, M. K., Singh, P. K., and Singh, V.: An assessment of global satellite-based precipitation datasets in capturing precipitation extremes: A comparison with observed precipitation dataset in India, International Journal of Climatology, 40, 3667–3688, https://doi.org/10.1002/joc.6419, 2020.

Harris, J. M., Draxler, R. R., and Oltmans, S. J.: Trajectory model sensitivity to differences in input data and vertical transport method, J. Geophys. Res.-Atmos., 110, D14109, https://doi.org/10.1029/2004JD005750, 2005.

Hilario, M. R. A., Olaguera, L. M., Narisma, G. T., and Matsumoto, J.: Diurnal Characteristics of Summer Precipitation Over Luzon Island, Philippines, Asia-Pacific J Atmos Sci, https://doi.org/10.1007/s13143-020-00214-1, 2020.

Hilario, M. R. A., Crosbie, E., Shook, M., Reid, J. S., Cambaliza, M. O. L., Simpas, J. B. B., Ziemba, L., DiGangi, J. P., Diskin, G. S., Nguyen, P., Turk, F. J., Winstead, E., Robinson, C. E., Wang, J., Zhang, J., Wang, Y., Yoon, S., Flynn, J., Alvarez, S. L., Behrangi, A., and Sorooshian, A.: Measurement report: Long-range transport patterns into the tropical northwest Pacific during the CAMP^{2}Ex aircraft campaign: chemical composition, size distributions, and the impact of convection, Atmospheric Chemistry and Physics, 21, 3777–3802, https://doi.org/10.5194/acp-21-3777-2021, 2021.

Hilario, M. R. A., Bañaga, P. A., Betito, G., Braun, R. A., Cambaliza, M. O., Cruz, M. T., Lorenzo, G. R., MacDonald, A. B., Pabroa, P. C., Simpas, J. B., Stahl, C., Yee, J. R., and Sorooshian, A.: Stubborn aerosol: why particulate mass concentrations do not drop during the wet season in Metro Manila, Philippines, Environ. Sci.: Atmos., 2, 1428–1437, https://doi.org/10.1039/D2EA00073C, 2022.

Hodzic, A., Kasibhatla, P. S., Jo, D. S., Cappa, C. D., Jimenez, J. L., Madronich, S., and Park, R. J.: Rethinking the global secondary organic aerosol (SOA) budget: stronger production, faster removal, shorter lifetime, Atmospheric Chemistry and Physics, 16, 7917–7941, https://doi.org/10.5194/acp-16-7917-2016, 2016.

Hoesly, R. M., Smith, S. J., Feng, L., Klimont, Z., Janssens-Maenhout, G., Pitkanen, T., Seibert, J. J., Vu, L., Andres, R. J., Bolt, R. M., Bond, T. C., Dawidowski, L., Kholod, N., Kurokawa, J., Li, M., Liu, L., Lu, Z., Moura, M. C. P., O'Rourke, P. R., and Zhang, Q.: Historical (1750–2014) anthropogenic emissions of reactive gases and aerosols from the Community Emissions Data System (CEDS), Geoscientific Model Development, 11, 369–408, https://doi.org/10.5194/gmd-11-369-2018, 2018.

Hou, P., Wu, S., McCarty, J. L., and Gao, Y.: Sensitivity of atmospheric aerosol scavenging to precipitation intensity and frequency in the context of global climate change, Atmospheric Chemistry and Physics, 18, 8173–8182, https://doi.org/10.5194/acp-18-8173-2018, 2018.

Huffman, G. J., Bolvin, D. T., Braithwaite, D., Hsu, K.-L., Joyce, R. J., Kidd, C., Nelkin, E. J., Sorooshian, S., Stocker, E. F., Tan, J., Wolff, D. B., and Xie, P.: Integrated Multi-satellite Retrievals for the Global Precipitation Measurement (GPM) Mission (IMERG), in: Satellite Precipitation Measurement: Volume 1, edited by: Levizzani, V., Kidd, C., Kirschbaum, D. B., Kummerow, C. D., Nakamura, K., and Turk, F. J., Springer International Publishing, Cham, 343–353, https://doi.org/10.1007/978-3-030-24568-9_19, 2020.

Jalkanen, J.-P., Johansson, L., Kukkonen, J., Brink, A., Kalli, J., and Stipa, T.: Extension of an assessment model of ship traffic exhaust emissions for particulate matter and carbon monoxide, Atmospheric Chemistry and Physics, 12, 2641–2659, https://doi.org/10.5194/acp-12-2641-2012, 2012.

Jensen, J. B. and Charlson, R. J.: On the efficiency of nucleation scavenging, Tellus B, 36B, 367–375, https://doi.org/10.1111/j.1600-0889.1984.tb00255.x, 1984.

Jiang, Q., Li, W., Fan, Z., He, X., Sun, W., Chen, S., Wen, J., Gao, J., and Wang, J.: Evaluation of the ERA5 reanalysis precipitation dataset over Chinese Mainland, Journal of Hydrology, 595, 125660, https://doi.org/10.1016/j.jhydrol.2020.125660, 2021.

Kanaya, Y., Pan, X., Miyakawa, T., Komazaki, Y., Taketani, F., Uno, I., and Kondo, Y.: Long-term observations of black carbon mass concentrations at Fukue Island, western Japan, during 2009–2015: constraining wet removal rates and emission strengths from East Asia, Atmospheric Chemistry and Physics, 16, 10689–10705, https://doi.org/10.5194/acp-16-10689-2016, 2016.

Kanaya, Y., Yamaji, K., Miyakawa, T., Taketani, F., Zhu, C., Choi, Y., Komazaki, Y., Ikeda, K., Kondo, Y., and Klimont, Z.: Rapid reduction in black carbon emissions from China: evidence from 2009–2019 observations on Fukue Island, Japan, Atmospheric Chemistry and Physics, 20, 6339–6356, https://doi.org/10.5194/acp-20-6339-2020, 2020.

Kidd, C., Graham, E., Smyth, T., and Gill, M.: Assessing the Impact of Light/Shallow Precipitation Retrievals from Satellite-Based Observations Using Surface Radar and Micro Rain Radar Observations, Remote Sensing, 13, 1708, https://doi.org/10.3390/rs13091708, 2021.

Kim, K. D., Lee, S., Kim, J.-J., Lee, S.-H., Lee, D., Lee, J.-B., Choi, J.-Y., and Kim, M. J.: Effect of Wet Deposition on Secondary Inorganic Aerosols Using an Urban-Scale Air Quality Model, Atmosphere, 12, 168, https://doi.org/10.3390/atmos12020168, 2021.

Kipling, Z., Stier, P., Johnson, C. E., Mann, G. W., Bellouin, N., Bauer, S. E., Bergman, T., Chin, M., Diehl, T., Ghan, S. J., Iversen, T., Kirkevåg, A., Kokkola, H., Liu, X., Luo, G., van Noije, T., Pringle, K. J., von Salzen, K., Schulz, M., Seland, Ø., Skeie, R. B., Takemura, T., Tsigaridis, K., and Zhang, K.: What controls the vertical distribution of aerosol? Relationships between process sensitivity in HadGEM3–UKCA and inter-model variation from AeroCom Phase II, Atmos. Chem. Phys., 16, 2221–2241, https://doi.org/10.5194/acp-16-2221-2016, 2016.

Kleinman, L. I., Daum, P. H., Lee, Y.-N., Senum, G. I., Springston, S. R., Wang, J., Berkowitz, C., Hubbe, J., Zaveri, R. A., Brechtel, F. J., Jayne, J., Onasch, T. B., and Worsnop, D.: Aircraft observations of aerosol composition and ageing in New England and Mid-Atlantic States during the summer 2002 New England Air Quality Study field campaign, J. Geophys. Res., 112, D09310, https://doi.org/10.1029/2006JD007786, 2007.

Kohavi, R.: A study of cross-validation and bootstrap for accuracy estimation and model selection, in: Proceedings of the 14th international joint conference on Artificial intelligence - Volume 2, San Francisco, CA, USA, 1137–1143, 1995.

Koike, M., Kondo, Y., Kita, K., Takegawa, N., Masui, Y., Miyazaki, Y., Ko, M. W., Weinheimer, A. J., Flocke, F., Weber, R. J., Thornton, D. C., Sachse, G. W., Vay, S. A., Blake, D. R., Streets, D. G., Eisele, F. L., Sandholm, S. T., Singh, H. B., and Talbot, R. W.: Export of anthropogenic reactive nitrogen and sulfur compounds from the East Asia region in spring, J. Geophys. Res., 108, 8789, https://doi.org/10.1029/2002JD003284, 2003.

Kondo, Y., Matsui, H., Moteki, N., Sahu, L., Takegawa, N., Kajino, M., Zhao, Y., Cubison, M. J., Jimenez, J. L., Vay, S., Diskin, G. S., Anderson, B., Wisthaler, A., Mikoviny, T., Fuelberg, H. E., Blake, D. R., Huey, G., Weinheimer, A. J., Knapp, D. J., and Brune, W. H.: Emissions of black carbon, organic, and inorganic aerosols from biomass burning in North America and Asia in 2008, J. Geophys. Res., 116, D08204, https://doi.org/10.1029/2010JD015152, 2011.

Lack, D. A. and Corbett, J. J.: Black carbon from ships: a review of the effects of ship speed, fuel quality and exhaust gas scrubbing, Atmospheric Chemistry and Physics, 12, 3985–4000, https://doi.org/10.5194/acp-12-3985-2012, 2012.

Lin, C., Huo, T., Yang, F., Wang, B., Chen, Y., and Wang, H.: Characteristics of Water-soluble Inorganic Ions in Aerosol and Precipitation and their Scavenging Ratios in an Urban Environment in Southwest China, Aerosol Air Qual. Res., 21, 200513, https://doi.org/10.4209/aaqr.200513, 2021.

Liu, D., Allan, J., Whitehead, J., Young, D., Flynn, M., Coe, H., McFiggans, G., Fleming, Z. L., and Bandy, B.: Ambient black carbon particle hygroscopic properties controlled by mixing state and composition, Atmospheric Chemistry and Physics, 13, 2015–2029, https://doi.org/10.5194/acp-13-2015-2013, 2013.

Liu, M. and Matsui, H.: Improved Simulations of Global Black Carbon Distributions by Modifying Wet Scavenging Processes in Convective and Mixed-Phase Clouds, Journal of Geophysical Research: Atmospheres, 126, e2020JD033890, https://doi.org/10.1029/2020JD033890, 2021.

Livingston, J. M., Schmid, B., Russell, P. B., Podolske, J. R., Redemann, J., and Diskin, G. S.: Comparison of Water Vapor Measurements by Airborne Sun Photometer and Diode Laser Hygrometer on the NASA DC-8, Journal of Atmospheric and Oceanic Technology, 25, 1733–1743, https://doi.org/10.1175/2008JTECHA1047.1, 2008.

Lu, X. C. and Fung, J. C. H.: Sensitivity assessment of PM2.5 simulation to the below-cloud washout schemes in an atmospheric chemical transport model, Tellus B: Chemical and Physical Meteorology, 70, 1–17, https://doi.org/10.1080/16000889.2018.1476435, 2018.

Luo, G., Yu, F., and Schwab, J.: Revised treatment of wet scavenging processes dramatically improves GEOS-Chem 12.0.0 simulations of surface nitric acid, nitrate, and ammonium over the United States, Geoscientific Model Development, 12, 3439–3447, https://doi.org/10.5194/gmd-12-3439-2019, 2019.

MacDonald, A. B., Dadashazar, H., Chuang, P. Y., Crosbie, E., Wang, H., Wang, Z., Jonsson, H. H., Flagan, R. C., Seinfeld, J. H., and Sorooshian, A.: Characteristic Vertical Profiles of Cloud Water Composition in Marine Stratocumulus Clouds and Relationships With Precipitation, J. Geophys. Res. Atmos., 123, 3704–3723, https://doi.org/10.1002/2017JD027900, 2018.

Mahmood, R., von Salzen, K., Flanner, M., Sand, M., Langner, J., Wang, H., and Huang, L.: Seasonality of global and Arctic black carbon processes in the Arctic Monitoring and Assessment Programme models, Journal of Geophysical Research: Atmospheres, 121, 7100–7116, https://doi.org/10.1002/2016JD024849, 2016.

Marinescu, P. J., Heever, S. C. van den, Saleeby, S. M., Kreidenweis, S. M., and DeMott, P. J.: The Microphysical Roles of Lower-Tropospheric versus Midtropospheric Aerosol Particles in Mature-Stage MCS Precipitation, Journal of the Atmospheric Sciences, 74, 3657–3678, https://doi.org/10.1175/JAS-D-16-0361.1, 2017.

Matsui, H., Kondo, Y., Moteki, N., Takegawa, N., Sahu, L. K., Zhao, Y., Fuelberg, H. E., Sessions, W. R., Diskin, G., Blake, D. R., Wisthaler, A., and Koike, M.: Seasonal variation of the transport of black carbon aerosol from the Asian continent to the Arctic during the ARCTAS aircraft campaign, J. Geophys. Res., 116, D05202, https://doi.org/10.1029/2010JD015067, 2011.

Mitra, S. K., Brinkmann, J., and Pruppacher, H. R.: A wind tunnel study on the drop-to-particle conversion, Journal of Aerosol Science, 23, 245–256, https://doi.org/10.1016/0021-8502(92)90326-Q, 1992.

Moteki, N. and Kondo, Y.: Effects of Mixing State on Black Carbon Measurements by Laser-Induced Incandescence, Aerosol Science and Technology, 41, 398–417, https://doi.org/10.1080/02786820701199728, 2007.

Moteki, N. and Kondo, Y.: Dependence of Laser-Induced Incandescence on Physical Properties of Black Carbon Aerosols: Measurements and Theoretical Interpretation, Aerosol Science and Technology, 44, 663–675, https://doi.org/10.1080/02786826.2010.484450, 2010.

Moteki, N., Kondo, Y., Oshima, N., Takegawa, N., Koike, M., Kita, K., Matsui, H., and Kajino, M.: Size dependence of wet removal of black carbon aerosols during transport from the boundary layer to the free troposphere, Geophys. Res. Lett., 39, L13802, https://doi.org/10.1029/2012GL052034, 2012.

Moteki, N., Mori, T., Matsui, H., and Ohata, S.: Observational constraint of in-cloud supersaturation for simulations of aerosol rainout in atmospheric models, npj Clim Atmos Sci, 2, 1–11, https://doi.org/10.1038/s41612-019-0063-y, 2019.

Murphy, D. M., Cziczo, D. J., Hudson, P. K., Thomson, D. S., Wilson, J. C., Kojima, T., and Buseck, P. R.: Particle Generation and Resuspension in Aircraft Inlets when Flying in Clouds, Aerosol Science and Technology, 38, 401–409, https://doi.org/10.1080/02786820490443094, 2004.

Nadeem, M. U., Anjum, M. N., Afzal, A., Azam, M., Hussain, F., Usman, M., Javaid, M. M., Mukhtar, M. A., and Majeed, F.: Assessment of Multi-Satellite Precipitation Products over the Himalayan Mountains of Pakistan, South Asia, Sustainability, 14, 8490, https://doi.org/10.3390/su14148490, 2022.

Nguyen, P., Ombadi, M., Sorooshian, S., Hsu, K., AghaKouchak, A., Braithwaite, D., Ashouri, H., and Thorstensen, A. R.: The PERSIANN family of global satellite precipitation data: a review and evaluation of products, Hydrol. Earth Syst. Sci., 22, 5801–5816, https://doi.org/10.5194/hess-22-5801-2018, 2018.

Nicholson, S. E., Klotter, D., Zhou, L., and Hua, W.: Validation of Satellite Precipitation Estimates over the Congo Basin, J. Hydrometeor., 20, 631–656, https://doi.org/10.1175/JHM-D-18-0118.1, 2019.

Oshima, N., Kondo, Y., Moteki, N., Takegawa, N., Koike, M., Kita, K., Matsui, H., Kajino, M., Nakamura, H., Jung, J. S., and Kim, Y. J.: Wet removal of black carbon in Asian outflow: Aerosol Radiative Forcing in East Asia (A-FORCE) aircraft campaign, J. Geophys. Res., 117, n/a-n/a, https://doi.org/10.1029/2011JD016552, 2012.

Radke, L. F., Hobbs, P. V., and Eltgroth, M. W.: Scavenging of Aerosol Particles by Precipitation, Journal of Applied Meteorology and Climatology, 19, 715–722, https://doi.org/10.1175/1520-0450(1980)019<0715:SOAPBP>2.0.CO;2, 1980.

Reid, J. S., Maring, H. B., Narisma, G. T., Heever, S. van den, Girolamo, L. D., Ferrare, R., Lawson, P., Mace, G. G., Simpas, J. B., Tanelli, S., Ziemba, L., Diedenhoven, B. van, Bruintjes, R., Bucholtz, A., Cairns, B., Cambaliza, M. O., Chen, G., Diskin, G. S., Flynn, J. H., Hostetler, C. A., Holz, R. E., Lang, T. J., Schmidt, K. S., Smith, G., Sorooshian, A., Thompson, E. J., Thornhill, K. L., Trepte, C., Wang, J., Woods, S., Yoon, S., Alexandrov, M., Alvarez, S., Amiot, C. G., Bennett, J. R., M., B., Burton, S. P., Cayanan, E., Chen, H., Collow, A., Crosbie, E., DaSilva, A., DiGangi, J. P., Flagg, D. D., Freeman, S. W., Fu, D., Fukada, E., Hilario, M. R. A., Hong, Y., Hristova-Veleva, S. M., Kuehn, R., Kowch, R. S., Leung, G. R., Loveridge, J., Meyer, K., Miller, R. M., Montes, M. J., Moum, J. N., Nenes, T., Nesbitt, S. W., Norgren, M., Nowottnick, E. P., Rauber, R. M., Reid, E. A., Rutledge, S., Schlosser, J. S., Sekiyama, T. T., Shook, M. A., Sokolowsky, G. A., Stamnes, S. A., Tanaka, T. Y., Wasilewski, A., Xian, P., Xiao, Q., Xu, Z., and Zavaleta, J.: The coupling between tropical meteorology, aerosol lifecycle, convection, and radiation, during the Cloud, Aerosol and Monsoon Processes Philippines Experiment (CAMP2Ex), Bulletin of the American Meteorological Society, 1, https://doi.org/10.1175/BAMS-D-21-0285.1, 2023.

Rolph, G., Stein, A., and Stunder, B.: Real-time Environmental Applications and Display sYstem: READY, Environmental Modelling & Software, 95, 210–228, https://doi.org/10.1016/j.envsoft.2017.06.025, 2017.

Ryu, Y.-H. and Min, S.-K.: Improving Wet and Dry Deposition of Aerosols in WRF-Chem: Updates to Below-Cloud Scavenging and Coarse-Particle Dry Deposition, Journal of Advances in Modeling Earth Systems, 14, e2021MS002792, https://doi.org/10.1029/2021MS002792, 2022.

Ryu, Y.-H., Min, S.-K., and Knote, C.: Contrasting roles of clouds as a sink and source of aerosols: A quantitative assessment using WRF-Chem over East Asia, Atmospheric Environment, 277, 119073, https://doi.org/10.1016/j.atmosenv.2022.119073, 2022.

Samset, B. H., Myhre, G., Schulz, M., Balkanski, Y., Bauer, S., Berntsen, T. K., Bian, H., Bellouin, N., Diehl, T., Easter, R. C., Ghan, S. J., Iversen, T., Kinne, S., Kirkevåg, A., Lamarque, J.-F., Lin, G., Liu, X., Penner, J. E., Seland, Ø., Skeie, R. B., Stier, P., Takemura, T., Tsigaridis, K., and Zhang, K.: Black carbon vertical profiles strongly affect its radiative forcing uncertainty, Atmospheric Chemistry and Physics, 13, 2423–2434, https://doi.org/10.5194/acp-13-2423-2013, 2013.

Sapiano, M. R. P. and Arkin, P. A.: An Intercomparison and Validation of High-Resolution Satellite Precipitation Estimates with 3-Hourly Gauge Data, Journal of Hydrometeorology, 10, 149–166, https://doi.org/10.1175/2008JHM1052.1, 2009.

Seinfeld, J. H. and Pandis, S. N.: Atmospheric Chemistry and Physics: From Air Pollution to Climate Change, Third., John Wiley & Sons, Inc, New Jersey, 2016.

Shen, Z., Ming, Y., Horowitz, L. W., Ramaswamy, V., and Lin, M.: On the Seasonality of Arctic Black Carbon, Journal of Climate, 30, 4429–4441, https://doi.org/10.1175/JCLI-D-16-0580.1, 2017.

Slowik, J. G., Cross, E. S., Han, J.-H., Davidovits, P., Onasch, T. B., Jayne, J. T., Williams, L. R., Canagaratna, M. R., Worsnop, D. R., Chakrabarty, R. K., Moosmüller, H., Arnott, W. P., Schwarz, J. P., Gao, R.-S., Fahey, D. W., Kok, G. L., and Petzold, A.: An Inter-Comparison of Instruments Measuring Black Carbon Content of Soot Particles, Aerosol Science and Technology, 41, 295–314, https://doi.org/10.1080/02786820701197078, 2007.

Soulie, A., Granier, C., Darras, S., Zilbermann, N., Doumbia, T., Guevara, M., Jalkanen, J.-P., Keita, S., Liousse, C., Crippa, M., Guizzardi, D., Hoesly, R., and Smith, S.: Global Anthropogenic Emissions (CAMS-GLOB-ANT) for the Copernicus Atmosphere Monitoring Service Simulations of Air Quality Forecasts and Reanalyses, Earth System Science Data Discussions, 1–45, https://doi.org/10.5194/essd-2023-306, 2023.

Stahl, C., Crosbie, E., Bañaga, P. A., Betito, G., Braun, R. A., Cainglet, Z. M., Cambaliza, M. O., Cruz, M. T., Dado, J. M., Hilario, M. R. A., Leung, G. F., MacDonald, A. B., Magnaye, A. M., Reid, J., Robinson, C., Shook, M. A., Simpas, J. B., Visaga, S. M., Winstead, E., Ziemba, L., and Sorooshian, A.: Total organic carbon and the contribution from speciated organics in cloud water: airborne data analysis from the CAMP^{2}Ex field campaign, Atmospheric Chemistry and Physics, 21, 14109–14129, https://doi.org/10.5194/acp-21-14109-2021, 2021.

Stein, A. F., Draxler, R. R., Rolph, G. D., Stunder, B. J. B., Cohen, M. D., and Ngan, F.: NOAA's HYSPLIT Atmospheric Transport and Dispersion Modeling System, Bull. Amer. Meteor. Soc., 96, 2059–2077, https://doi.org/10.1175/BAMS-D-14-00110.1, 2015.

Stockwell, C. E., Veres, P. R., Williams, J., and Yokelson, R. J.: Characterization of biomass burning emissions from cooking fires, peat, crop residue, and other fuels with high-resolution proton-transfer-reaction time-of-flight mass spectrometry, Atmos. Chem. Phys., 15, 845–865, https://doi.org/10.5194/acp-15-845-2015, 2015.

Textor, C., Schulz, M., Guibert, S., Kinne, S., Balkanski, Y., Bauer, S., Berntsen, T., Berglen, T., Boucher, O., Chin, M., Dentener, F., Diehl, T., Easter, R., Feichter, H., Fillmore, D., Ghan, S., Ginoux, P., Gong, S., Grini, A., Hendricks, J., Horowitz, L., Huang, P., Isaksen, I., Iversen, I., Kloster, S., Koch, D., Kirkevåg, A., Kristjansson, J. E., Krol, M., Lauer, A., Lamarque, J. F., Liu, X., Montanaro, V., Myhre, G., Penner, J., Pitari, G., Reddy, S., Seland, Ø., Stier, P., Takemura, T., and Tie, X.: Analysis and quantification of the diversities of aerosol life cycles within AeroCom, Atmospheric Chemistry and Physics, 6, 1777–1813, https://doi.org/10.5194/acp-6-1777-2006, 2006.

Wang, J., Petersen, W. A., and Wolff, D. B.: Validation of Satellite-Based Precipitation Products from TRMM to GPM, Remote Sensing, 13, 1745, https://doi.org/10.3390/rs13091745, 2021a.

Wang, X., Zhang, L., and Moran, M. D.: Uncertainty assessment of current size-resolved parameterizations for below-cloud particle scavenging by rain, Atmospheric Chemistry and Physics, 10, 5685–5705, https://doi.org/10.5194/acp-10-5685-2010, 2010.

Wang, X., Zhang, L., and Moran, M. D.: On the discrepancies between theoretical and measured below-cloud particle scavenging coefficients for rain – a numerical investigation using a detailed one-dimensional cloud microphysics model, Atmospheric Chemistry and Physics, 11, 11859–11866, https://doi.org/10.5194/acp-11-11859-2011, 2011.

Wang, X., Zhang, L., and Moran, M. D.: Bulk or modal parameterizations for below-cloud scavenging of fine, coarse, and giant particles by both rain and snow, Journal of Advances in Modeling Earth Systems, 6, 1301–1310, https://doi.org/10.1002/2014MS000392, 2014a.

Wang, X., Zhang, L., and Moran, M. D.: Development of a new semi-empirical parameterization for below-cloud scavenging of size-resolved aerosol particles by both rain and snow, Geoscientific Model Development, 7, 799–819, https://doi.org/10.5194/gmd-7-799-2014, 2014b.

Wang, Y., You, Y., and Kulie, M.: Global Virga Precipitation Distribution Derived From Three Spaceborne Radars and Its Contribution to the False Radiometer Precipitation Detection, Geophysical Research Letters, 45, 4446–4455, https://doi.org/10.1029/2018GL077891, 2018.

Wang, Y., Xia, W., Liu, X., Xie, S., Lin, W., Tang, Q., Ma, H.-Y., Jiang, Y., Wang, B., and Zhang, G. J.: Disproportionate control on aerosol burden by light rain, Nat. Geosci., 14, 72–76, https://doi.org/10.1038/s41561-020-00675-z, 2021b.

Wang, Y., Xia, W., and Zhang, G. J.: What rainfall rates are most important to wet removal of different aerosol types?, Atmospheric Chemistry and Physics Discussions, 1–33, https://doi.org/10.5194/acp-2021-542, 2021c.

Watson-Parris, D., Schutgens, N., Reddington, C., Pringle, K. J., Liu, D., Allan, J. D., Coe, H., Carslaw, K. S., and Stier, P.: In-situ constraints on the vertical distribution of global aerosol, Aerosols/Atmospheric Modelling/Troposphere/Physics (physical properties and processes), https://doi.org/10.5194/acp-2018-1337, 2019.

Xian, P., Reid, J. S., Atwood, S. A., Johnson, R. S., Hyer, E. J., Westphal, D. L., and Sessions, W.: Smoke aerosol transport patterns over the Maritime Continent, Atmospheric Research, 122, 469–485, https://doi.org/10.1016/j.atmosres.2012.05.006, 2013.

Xu, D., Ge, B., Chen, X., Sun, Y., Cheng, N., Li, M., Pan, X., Ma, Z., Pan, Y., and Wang, Z.: Multi-method determination of the below-cloud wet scavenging coefficients of aerosols in Beijing, China, Atmospheric Chemistry and Physics, 19, 15569–15581, https://doi.org/10.5194/acp-19-15569-2019, 2019.

Xu, K.-M. and Randall, D. A.: A Semiempirical Cloudiness Parameterization for Use in Climate Models, Journal of the Atmospheric Sciences, 53, 3084–3102, https://doi.org/10.1175/1520-0469(1996)053<3084:ASCPFU>2.0.CO;2, 1996.

Zhang, W., Huang, A., Zhou, Y., Yang, B., Fang, D., Zhang, L., and Wu, Y.: Diurnal cycle of precipitation over Fujian Province during the pre-summer rainy season in southern China, Theor Appl Climatol, 130, 993–1006, https://doi.org/10.1007/s00704-016-1927-2, 2017.

Zhao, X., Sun, Y., Zhao, C., and Jiang, H.: Impact of Precipitation with Different Intensity on PM2.5 over Typical Regions of China, Atmosphere, 11, 906, https://doi.org/10.3390/atmos11090906, 2020.

Table 1: Examples of notation used in this study.

Predictor	**Description**	**Variations**
f_{RH95}	Fraction of hours along trajectories where GFS relative humidity (RH) > 95%	f_{RH85}, f_{RH90}
f_{MR15}	Fraction of hours along trajectories where GFS water vapor mixing ratio (MR) > 15 g kg^{-1} dry air	f_{MR17}
RH_{q95}	95th percentile of RH along trajectories	RH_{q50}, RH_{q85}, RH_{q90}, RH_{q100}, RH_{mean}
$RH_{w,\ DLH}$	RH over water measured by DLH onboard the aircraft	-
$APT_{PCP\ >\ 0.2\ mm,\ 48H,\ GFS,\ <\ 1500m}$	Accumulated precipitation calculated along 48-h trajectories where GFS precipitation is above 0.2 mm and trajectory altitude is below 1500 m	Trajectory duration: 12H, 24H, 48H, 72H Precipitation product: GFS, IMERG, PERSIANN-CDR Maximum altitude filter: no filter, < 1500 m Minimum precipitation filter: no filter, > 0.2 mm Other precipitation variables: PA, PF, PI

Formatted Table

Table 2: Curve-fitting equations considered where x is the predictor variable and y is the observed ΔBC/ΔCO while a, b, c, and d are best-fit parameters determined via least-squares regression.

Name	Equation	Source
Gaussian	$y = a \cdot \exp(-\frac{(x-b)^2}{2 \cdot c^2}) + d$	-
General Exponential	$y = a \cdot exp(-b \cdot x) + c$	-
Oshima	$y = b - a \cdot \log_{10}(x)$	Oshima et al. (2012)
Kanaya	$y = c \cdot exp(-a \cdot x^b)$	Kanaya et al. (2016)

Formatted Table

Formatted: Indent: First line: 0.25"

Formatted: Indent: First line: 0.25"

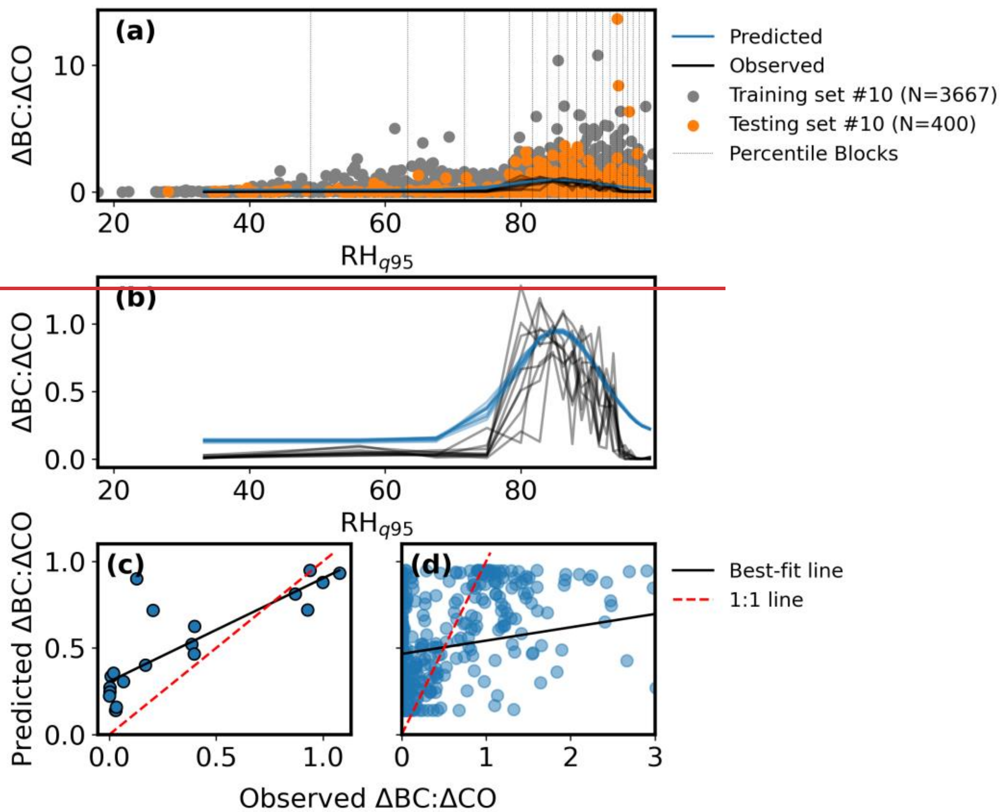

Formatted: Justified

~~(Hilario et al., 2021)~~

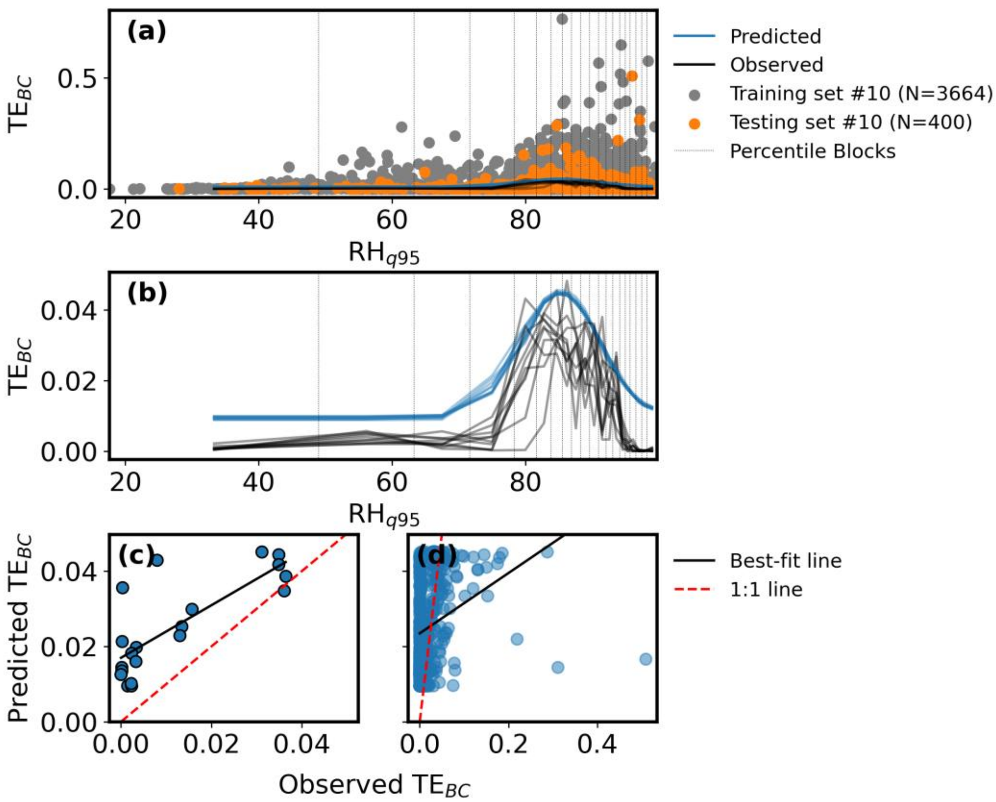

Figure 1: An example of the curve-fitting procedure on ~~ΔBC/ΔCO~~TE$_{BC}$ with RH$_{q95}$ as the predictor fitted with a G~~g~~aussian function. (a) Training (~~gray~~ gr~~a~~ey dots) and testing sets (orange dots) for the 10[th] iteration of the k-fold cross-validation procedure selected using stratified random sampling. Percentile blocks of each X-axis variable are denoted by vertical ~~gray~~ ~~grey~~gray lines with observed (black) and predicted curves (blue) also plotted for all 10 iterations. (b) Same as (a) but only showing observed (black) and predicted curves (blue) for all 10 iterations to highlight variations between the k iterations. (c) Scatterplot comparing RH$_{q95}$-predicted ΔBC/ΔCO and observed median TE$_{BC}$~~ΔBC/ΔCO~~ per 5th percentile block of the predictor. Note that (c) is simply the linear regression of the observed and predicted curves in (b). (d) Same as (c) but comparing RH$_{q95}$-predicted and observed TE$_{BC}$~~ΔBC/ΔCO~~ for individual points. In (c-d), only training set data are used, Y-axes are the same, the best-fit line is shown as a black line, and the 1:1 line is the red, dashed line.

Formatted: Subscript

Formatted: Subscript

Formatted: Subscript

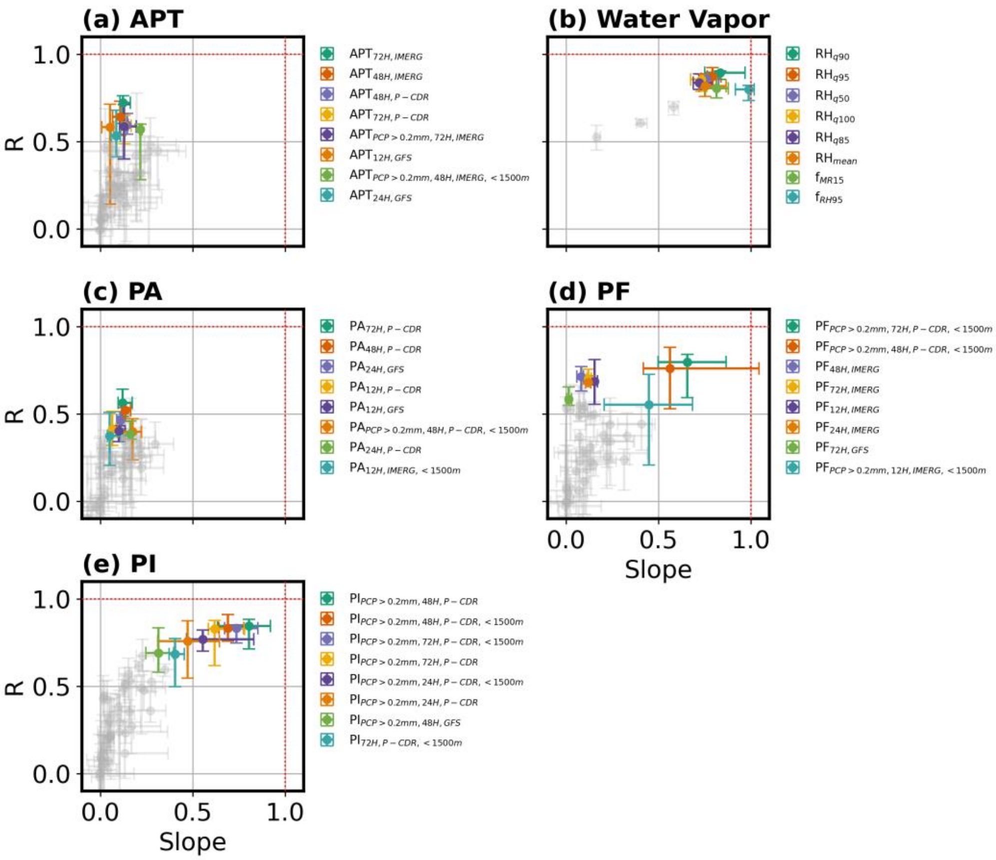
(a) APT
(b) Water Vapor
(c) PA
(d) PF
(e) PI
R
Slope
0.0
0.5
1.0
$APT_{72H, IMERG}$
$APT_{48H, IMERG}$
$APT_{48H, P-CDR}$
$APT_{72H, P-CDR}$
$APT_{PCP>0.2mm, 72H, IMERG}$
$APT_{12H, GFS}$
$APT_{PCP>0.2mm, 48H, IMERG, <1500m}$
$APT_{24H, GFS}$
RH_{q90}
RH_{q95}
RH_{q50}
RH_{q100}
RH_{q85}
RH_{mean}
f_{MR15}
f_{RH95}
$PA_{72H, P-CDR}$
$PA_{48H, P-CDR}$
$PA_{24H, GFS}$
$PA_{12H, P-CDR}$
$PA_{12H, GFS}$
$PA_{PCP>0.2mm, 48H, P-CDR, <1500m}$
$PA_{24H, P-CDR}$
$PA_{12H, IMERG, <1500m}$
$PF_{PCP>0.2mm, 72H, P-CDR, <1500m}$
$PF_{PCP>0.2mm, 48H, P-CDR, <1500m}$
$PF_{48H, IMERG}$
$PF_{72H, IMERG}$
$PF_{12H, IMERG}$
$PF_{24H, IMERG}$
$PF_{72H, GFS}$
$PF_{PCP>0.2mm, 12H, IMERG, <1500m}$
$PI_{PCP>0.2mm, 48H, P-CDR}$
$PI_{PCP>0.2mm, 48H, P-CDR, <1500m}$
$PI_{PCP>0.2mm, 72H, P-CDR, <1500m}$
$PI_{PCP>0.2mm, 72H, P-CDR}$
$PI_{PCP>0.2mm, 24H, P-CDR, <1500m}$
$PI_{PCP>0.2mm, 24H, P-CDR}$
$PI_{PCP>0.2mm, 48H, GFS}$
$PI_{72H, P-CDR, <1500m}$

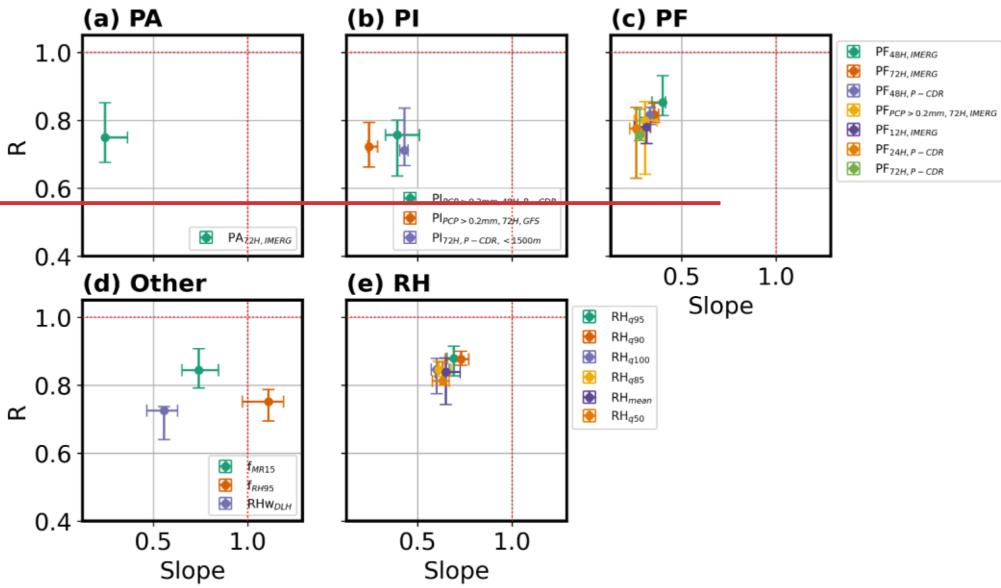

Figure 2: Slope and Pearson correlation (R) values derived from linear regressions of observed (x) and predicted (y) ~~ABC/ACO~~ TE$_{BC}$ with error bars representing the 25th and 75th percentile values derived from k-fold cross validation (k = 10) using stratified random sampling (Sect. 2.7~~5~~). Ideal values are denoted by the red dashed lines such that a better predictor would fall closer to the intersection of the two lines. Top eight predictors per group (panel) are colored non-gray while ~~Only p~~the rest of the predictors are plotted ~~redictors with median R > 0.70 are shown~~in gray to show the relative performance of all predictors. Note that PERSIANN-CDR has been abbreviated to P-CDR (b-c). Panels share the same X- and Y-axis limits.

Formatted: Subscript

Formatted: Not Highlight

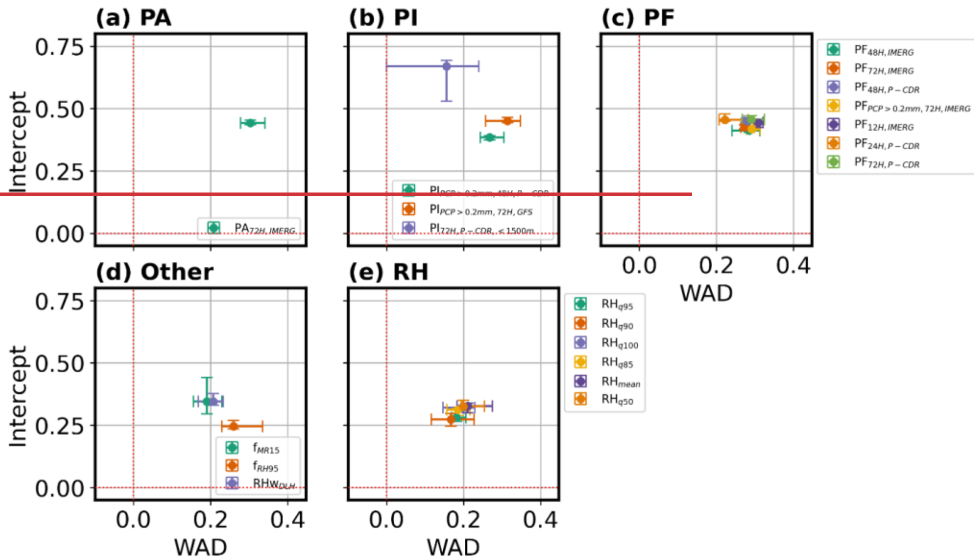

(a) PA
(b) PI
(c) PF
(d) Other
(e) RH
Intercept
WAD
0.75
0.50
0.25
0.00
0.0
0.2
0.4

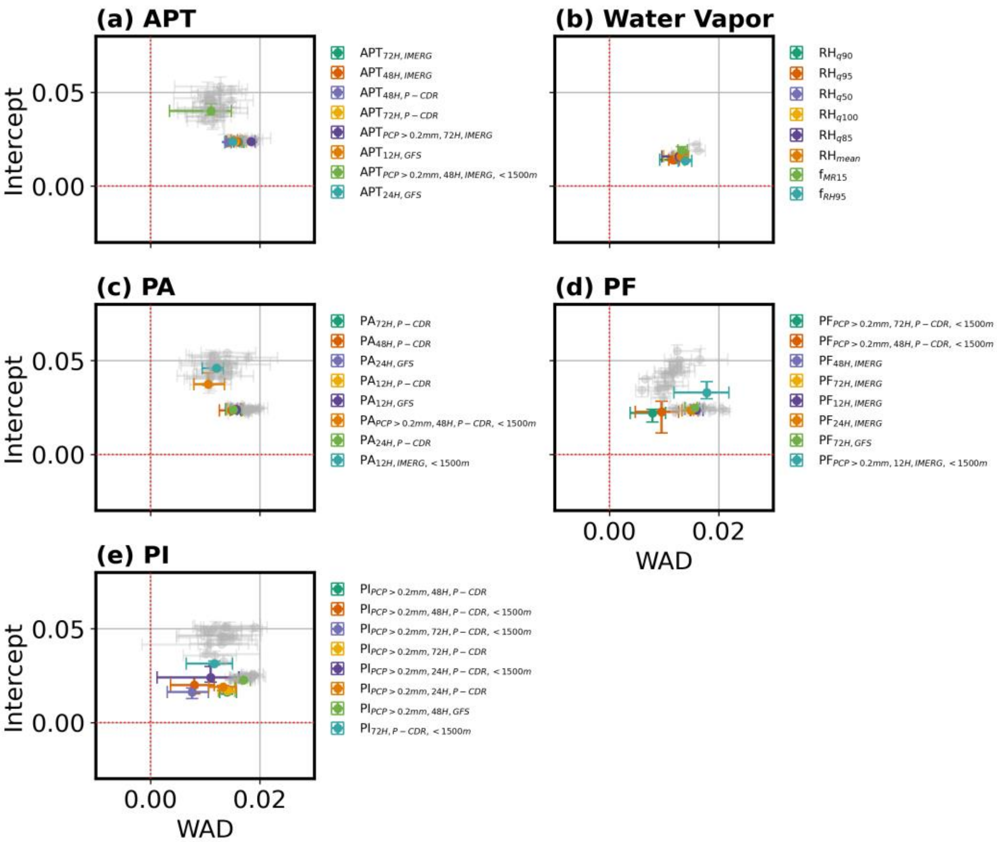

Figure 3: Same as Fig. 2 but comparing intercept and weighted area difference (WAD, Sect. 2.~~5~~7).

Formatted: Indent: First line: 0"

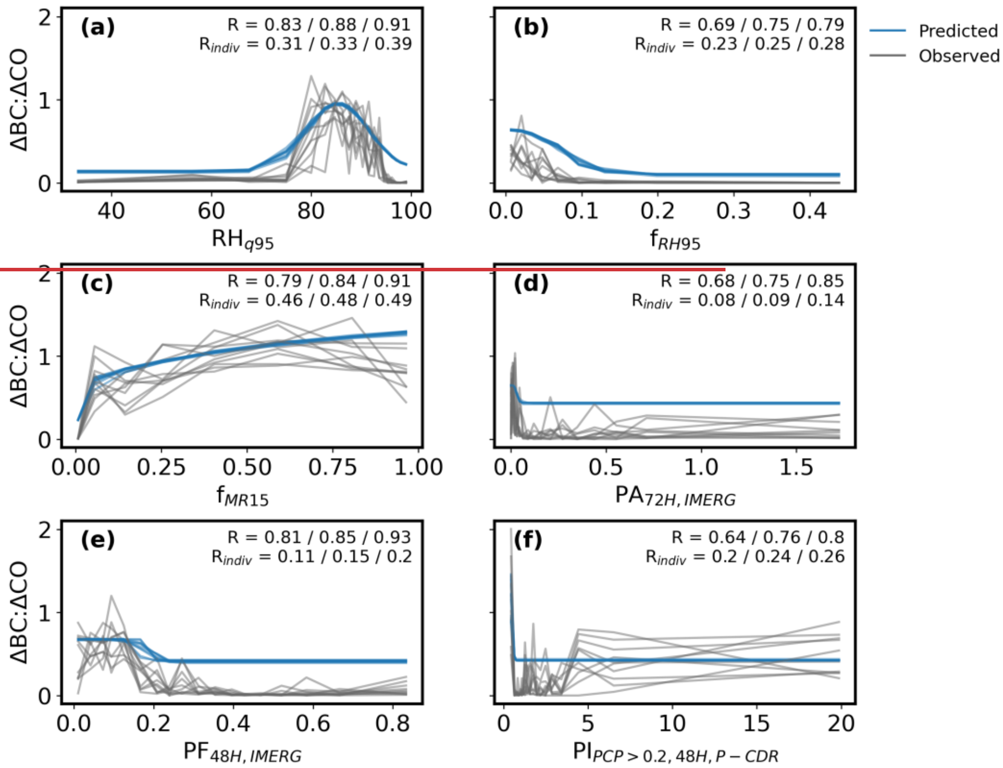

Formatted: Justified

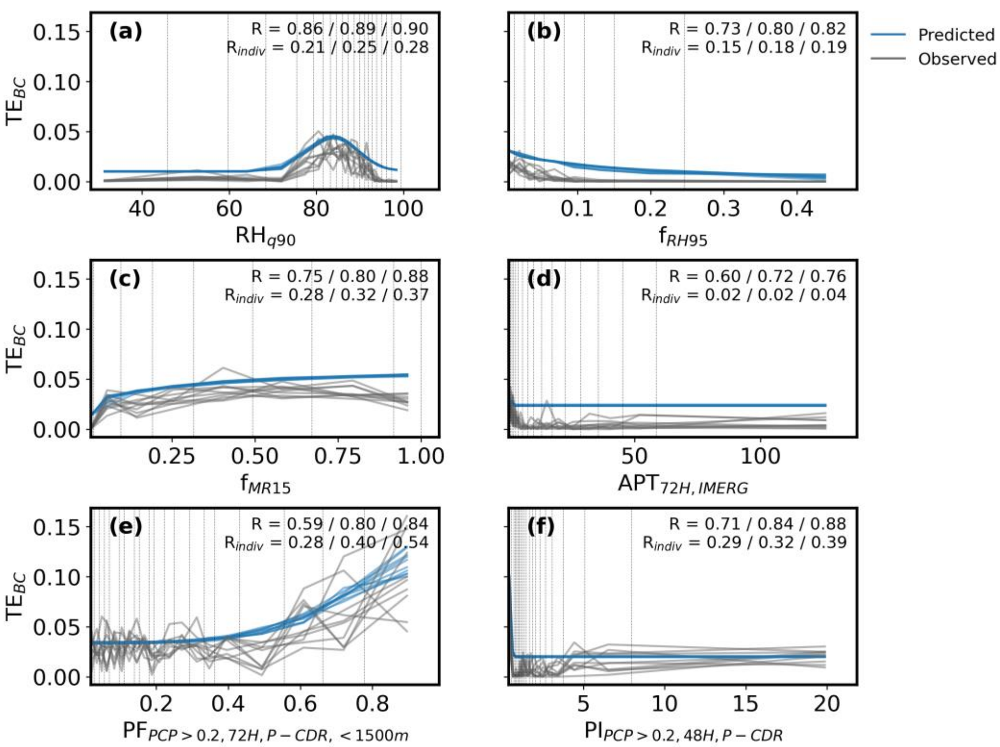

Figure 4: Median values of observed (black) and predicted ~~ABC/ACO~~TE$_{BC}$ (~~red~~blue) as a function of selected predictors for 10 iterations during k-fold cross-validation. Pearson correlations are annotated as 25th/50th/75th percentiles from k-fold iterations (k=10) calculated in two ways: comparing predicted and observed median TE$_{BC}$~~ABC/ACO~~ per 5th percentile block of the predictor (R) and comparing predicted and observed TE$_{BC}$~~ABC/ACO~~ for individual points (R$_{indiv}$). Panels share the same Y-axis limits. Percentile blocks for each ~~x~~X-axis variable are denoted by vertical gr~~a~~ey lines.

Formatted: Subscript

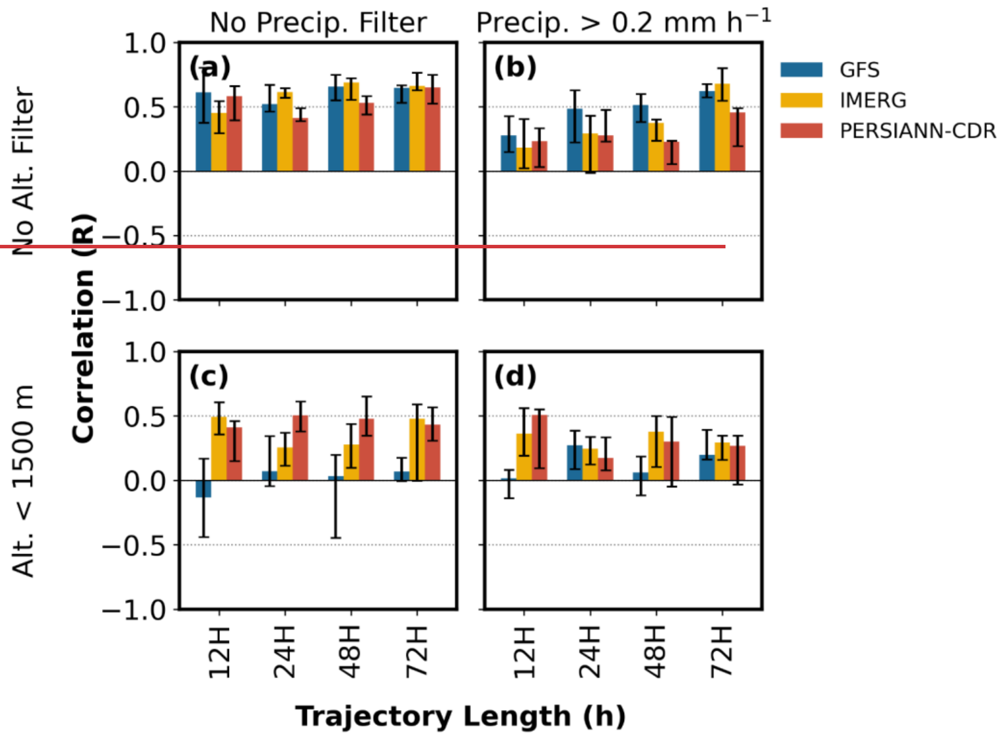
No Precip. Filter
Precip. > 0.2 mm h^{-1}
(a)
(b)
(c)
(d)
GFS
IMERG
PERSIANN-CDR
No Alt. Filter
Alt. < 1500 m
Correlation (R)
1.0
0.5
0.0
−0.5
−1.0
12H
24H
48H
72H
Trajectory Length (h)

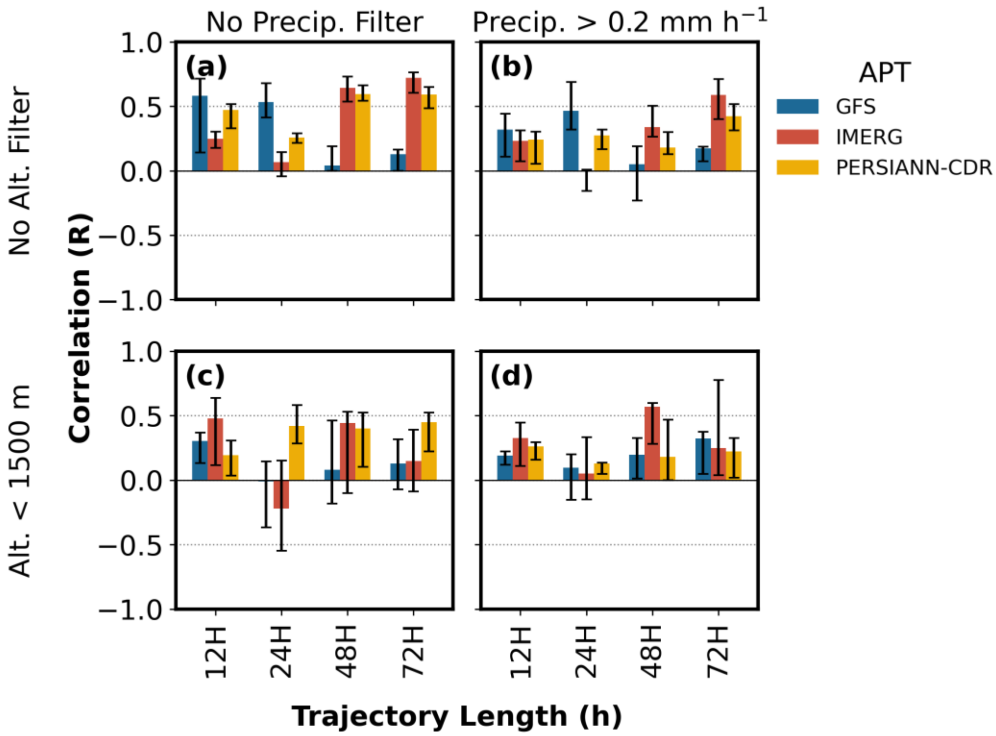

Figure 5: Pearson correlations (R) between observed ~~ABC/ACO~~TE_{BC} and ~~ABC/ACO~~ TE_{BC} predicted by accumulated precipitation along trajectories (APT) for different trajectory lengths and precipitation data products. Each panel refers to a combination of altitude and precipitation intensity filters. Panels share the same X- and Y-axis limits.

Formatted: Not Highlight

Formatted: Subscript, Not Highlight

Formatted: Subscript